THE JOURNAL OF BIOLOGICAL CHEMISTRY VOL. 290, NO. 11, pp. 6715–6730, March 13, 2015

Mechanisms Mediating Enhanced Neutralization Efficacy of Staphylococcal Enterotoxin B by Combinations of Monoclonal Antibodies*

Received for publication, December 9, 2014, and in revised form, January 6, 2015 Published, JBC Papers in Press, January 8, 2015, DOI 10.1074/jbc.M114.630715

Kaushik Dutta[‡1,2], **Avanish K. Varshney**[§¶1], **Matthew C. Franklin**[‡], **Michael Goger**[‡], **Xiaobo Wang**[¶], **and Bettina C. Fries**[§¶3]

From the [‡]*New York Structural Biology Center, New York, New York 10027, the* [§]*Department of Medicine and Molecular Genetics and Microbiology, Stony Brook University, Stony Brook, New York 11790, and the* [¶]*Department of Medicine, Microbiology and Immunology, Albert Einstein College of Medicine, Bronx, New York 10461*

Background: Staphylococcal enterotoxin B is a potent superantigen that causes lethal toxic shock syndrome.
Results: Ternary and binary complex of SEB with SEB specific mAbs identified three distinct epitopes.
Conclusion: Two different mechanisms illustrate how cocktails of mAbs enhance neutralization efficacy.
Significance: SEB neutralization via combination of mAbs is superior to monotherapy and can include non-neutralizing mAbs.

Staphylococcal enterotoxin B (SEB) is a superantigen that cross-links the major histocompatibility complex class II and specific V-β chains of the T-cell receptor, thus forming a ternary complex. Developing neutralizing mAb to disrupt the ternary complex and abrogate the resulting toxicity is a major therapeutic challenge because SEB is effective at very low concentrations. We show that combining two SEB-specific mAbs enhances their efficacy, even though one of the two mAbs by itself has no effect on neutralization. Crystallography was employed for fine-mapping conformational epitopes in binary and ternary complexes between SEB and Fab fragments. NMR spectroscopy was used to validate and identify subtle allosteric changes induced by mAbs binding to SEB. The mapping of epitopes established that a combination of different mAbs can enhance efficacy of mAb-mediated protection from SEB induced lethal shock by two different mechanisms: one mAb mixture promoted clearance of the toxin both *in vitro* and *in vivo* by FcR-mediated cross-linking and clearance, whereas the other mAb mixture induced subtle allosteric conformational changes in SEB that perturbed formation of the SEB·T-cell receptor·major histocompatibility complex class II trimer. Finally structural information accurately predicted mAb binding to other superantigens that share conformational epitopes with SEB. Fine mapping of conformational epitopes is a powerful tool to establish the mechanism and optimize the action of synergistic mAb combinations.

Staphylococcal enterotoxin B (SEB)[4] is classified as a category B agent by the Centers for Disease Control and Prevention, because of high toxicity, ease of production, and the potential to be aerosolized for wide dissemination. This toxin cross-links the major histocompatibility complex class II on antigen presenting cells and specific V-β variable domains of the T-cell receptor, resulting in a heterotrimeric complex. This ternary complex activates a large fraction of T lymphocytes (up to 20%), initiating a systemic release of proinflammatory cytokines (1, 2), which can result in a toxic shock syndrome (3). In the event of bioterrorism or accidental aerosol exposure to SEB, mAbs represent the only option for providing protective immunity to those who may be exposed to and need treatment of SEB intoxication. mAb treatment leads to the direct binding and neutralization of SEB. Antibody treatment to neutralize toxins was first reported in 1890 and has been routinely used to control disease progression with tetanus, snake bites, and scorpion stings (4–6). In 2009, a neutralizing mAb that binds the protective antigen component of *Bacillus anthracis* toxin was licensed by the Food and Drug Administration (7) for treatment of anthrax inhalation. Consequently more mAbs are being explored as therapies for other toxin-producing pathogens. In some cases, a combination of mAbs was required to achieve optimal protection (8–13). However, the administration of potent neutraliz-

* This work was supported, in whole or in part, by National Institutes of Health Grant U54 AI057158 (to B. C. F. and Prof. W. Ian Lipkin (Principal Investigator), Columbia University). This work was also supported by U.S. Department of Defense Grant W911NF0710053 (to the New York Structural Biology Center), a grant from New York Division of Science, Technology and Innovation, Office of Research Infrastructure Programs/National Institutes of Health facility improvement Grant CO6RR015495. The 900-MHz NMR spectrometers were purchased with funds from National Institutes of Health Grant P41GM066354, the Keck Foundation, New York State Assembly, and the U.S. Department of Defense. Use of the National Synchrotron Light Source, Brookhaven National Laboratory, was supported by the U.S. Department of Energy, Office of Science, Office of Basic Energy Sciences, under Contract DE-AC02-98CH10886.

The atomic coordinates and structure factors (codes 4RGM, 4RGN, and 4RGO) have been deposited in the Protein Data Bank (http://wwpdb.org/).

[1] Both authors contributed equally to this work.
[2] To whom correspondence may be addressed: New York Structural Biology Center, 89 Convent Avenue, New York, NY 10027. Tel.: 212-939-0660; Fax: 212-939-0863; E-mail: dutta@nysbc.org.
[3] To whom correspondence may be addressed: Molecular Genetics and Microbiology, HSC T 15, Rm. 080, Stony Brook, NY 11790. Tel.: 631-444-1901; Fax: 631-444-7518; E-mail: Bettina.Fries@stonybrookmedicine.edu.

[4] The abbreviations used are: SEB, staphylococcal enterotoxin B; SEC, staphylococcal enterotoxin C; TCR, T-cell receptor; PDB, Protein Data Bank; MHC-II, MHC class II; SEBILS, SEB-induced lethal shock; Fab, fragment antigen-binding; BLI, biolayer interferometry; HSQC, heteronuclear single quantum coherence; CRINEPT, cross-correlated relaxation-enhanced polarization transfer; FcR, Fc receptor; r.m.s.d., root mean square difference; SSA, streptococcal superantigen A; TROSY, transverse relaxation-optimized spectroscopy.

ing SEB-specific mAbs, either individually or as cocktails (14, 15), constitutes a challenge, because the onset of life-threatening symptoms after aerosol exposure occurs within 24 h (16). Given the short window for therapeutic intervention after exposure, lead clinical mAb candidates need to be optimized for postexposure treatment against SEB intoxication.

Previous studies in our laboratory have established two classes of mAbs that are neutralizing against the toxic effects of SEB exposure in murine models (17). The first class of mAbs provides effective protection when administered alone. The second class is nonprotective when administered singly; however, when administered in combination with a second SEB-specific mAb, the mixture provides effective protection similar to the first class of mAbs. Although several SEB neutralizing mAbs have been described (18–20), the precise mechanisms by which these antibodies prevent SEB-induced lethal shock (SEBILS) are largely unknown because of the lack of precise epitope mapping. Here we investigate the mechanisms of how single mAbs and their combination with the nonprotective mAbs enhance protective efficacy using both NMR and crystallography to determine the precise interactions between toxin and mAbs. We describe the x-ray crystal structures of SEB in complex with $20B1_{Fab}$, a neutralizing mAb, as well as SEB in complex with $6D3_{Fab}$ and $14G8_{Fab}$, two mAbs that are only protective in combination. This work is the first to describe the ternary complex of two fragment antigen-binding (Fab) domains and SEB using x-ray crystallography. We delineated the precise conformational epitopes on SEB to which each of the mAbs bind, thus explaining why mAb 20B1 is more potent at neutralizing SEB than either mAb 14G8 or mAb 6D3 when administered alone. We demonstrate that although promotion of FcR-mediated clearance is the mechanism by which enhanced efficacy is achieved in combination therapy with mAb 20B1 and nonprotective mAb 14G8, it does not explain the efficacy when the latter mAb is combined with mAb 6D3. For that mixture, NMR and biolayer interferometry data provide evidence that subtle allosteric conformational changes are induced in SEB through binding of mAbs, which might disrupt trimer formation. Furthermore, these data highlight that fine mapping of conformational epitopes can also identify shared epitopes among nonhomologous proteins and successfully predict cross-reactive antibodies.

EXPERIMENTAL PROCEDURES

Cloning and Purification of SEB—Recombinant full-length SEB (239 amino acids) was cloned into H-MBP-T vector (21) and purified as described earlier (17). Briefly, lysed cells were passed through an affinity column pre-equilibrated with the 20 mM Tris, pH 7.4. Protein was eluted with imidazole, and the fusion tag was cleaved by thrombin at 4 °C and subsequently passed through an ion exchange column. SEB fractions were pooled and further purified using a size exclusion column pre-equilibrated with NMR buffer (20 mM Tris, pH 7.5). NMR labeled samples were grown in M9 medium using either ^{15}N-labeled ammonium chloride and/or ^{13}C-labeled glucose as sole source for ^{15}N and ^{13}C isotopic labeling (Cambridge Isotope Laboratory). Purity of the protein was verified by SDS-PAGE. SEB was purchased from Toxin Technology (Sarasota, FL) in accordance with CDC biosafety regulations. All procedures were done in compliance with 42CFR parts 72 and 73 and health and safety regulations.

High Scale mAb and Fab Preparation—Three hybridoma cell lines producing murine SEB specific mAbs 20B1, 14G8, and 6D3 (17) were grown and purified as described previously (17). Fab fragments were generated from purified mAbs using a mouse IgG1 Fab preparation kit following the manufacturer's instructions (Thermo Scientific). Purity of the Fab fragments was confirmed by SDS-PAGE. For NMR and crystallography studies, unlabeled or labeled SEB was mixed with Fab fragments in 2:1 ratio, respectively. The excess SEB was removed by passage through a size exclusion column. The SEB·Fab complex fractions were pooled, concentrated, and used for crystallization.

Proliferation Assay—SEB induced proliferation was performed in mouse splenocytes and proliferation was measured using the ViaLight HS Cell Proliferation kit (Lonza), as previously described (17). SEB-specific mAbs (5 μg/ml) alone or in combination of mAbs (2.5 μg/ml of each mAb) were added concurrently with SEB (25 nM). Cells were incubated at 37 °C (22) with 10% CO_2 for 96 h.

Animal Experiments—All animal experiments were carried out in accordance with the rules and regulations of the Albert Einstein College of Medicine Animal Institute Committee. Protective efficacy against SEBILS was tested *in vivo* in mice. SEBILS was induced in mice by intraperitoneal injection of SEB (20 μg) and galactosamine (25 mg). For LPS-potentiating staphylococcal enterotoxin toxicity, mice were given SEB (5 μg) or SEC-1 (5 μg) intraperitoneal at 0 h, followed 3 h later by LPS (75 μg/mouse). Control mice received either staphylococcal enterotoxin or LPS alone. mAbs 20B1, 14G8, and 6D3 were given alone or in combinations 10 min prior to SEB, and the mice were observed for 5 days for their survival as described (17). In another set of experiments, SEB clearance from blood of mice ($n = 5$ per group) was analyzed by ELISA 6 h after the SEB challenge. GraphPad Prism 6 software was used to generate log rank survival curves.

SEB Clearance by Macrophages and Neutrophils—SEB uptake by macrophages was investigated using primary peritoneal macrophages. Primary peritoneal macrophages derived from WT C57/BL6 mice or FcR knockout ($FcR\gamma^{-/-}$/$RIIB^{-/-}$) mice of C57/BL6 background were harvested from mice 4 days after injecting 5 ml of 3% (w/v) brewer thioglycollate medium into the peritoneal cavity and resuspended (4×10^5/well) in 10% FBS/DMEM in a 96-well plate and incubated overnight at 37 °C with 10% CO_2 (22). Cells were treated with mAbs at the indicated dose either alone or in combination followed by SEB (5 μg/ml). Neutrophils were isolated from healthy human donor blood using standard method and treated with mAbs alone or in combination and then infected with SEB (5 μg/ml). Uptake of SEB by neutrophils or macrophages was studied by testing for depletion of SEB in supernatant by ELISA. These experiments were done in triplicate. Cross-reactivity of mAb 20B1 to other toxins (SEC1–3 and SSA) was investigated by standard ELISA as described previously (17).

Biolayer Interferometry (BLI): Direct Binding Assay—In compliance with select agent regulations (42CFR parts 72 and 73),

binding constant experiments were conducted using the Blitz instrument (ForteBio) at 25 °C. All tubes with the analyte and ligand were agitated at 2,000 rpm. Biotinylated SEB (Toxin Technology) was resuspended in 1× PBS to final concentration of 1 μM in 200 μl. Streptavidin biosensors were incubated in 1× PBS buffer for 10 min before the start of the experiment. Typical binding experiments was conducted as follows: prewash, in which the biosensor was incubated in 1× PBS buffer for 30 s; loading, in which the biosensor tip was immersed into the solution containing biotinylated SEB for 90 s, allowing biotinylated SEB to be immobilized onto the biosensor tip (typical capture levels were ~0.8 nm); baseline, in which the SEB immobilized biosensor tip was washed with 1× PBS for 30 s to remove all unbound biotinylated SEB; association, in which several different concentrations of the mAbs (20B1, 14G8, and 6D3 or mixed), MHC-II (hereafter called MHC), and/or TCR-β chain (hereafter called TCR) proteins were incubated with the immobilized SEB for 120 s depending on the specific assay (typical capture level varied from ~0.8 to 1.3 nm); and dissociation, during which the biosensor tip immobilized with SEB·ligand complex was dipped into 1× PBS for 120 s. The mAb concentrations that were used to determine binding affinities were 10, 20, 40, 60, 80, and 100 nM. A similar concentration range was used to determine the binding affinity of mAb 20B1 with SEC-1. The concentrations of TCR and MHC used to determine the binding affinity toward SEB were 4, 16, 32, 64, 128, and 164 μM and 0.4, 0.6, 0.8, 1.0, 1.2, 1.6, and 3.2 μM, respectively. Equilibrium dissociation constants were determined from the steady-state analysis of the BLI response at equilibrium (obtained after fitting the data) plotted as a function of ligand concentrations. All nonspecific binding to the biosensor were eliminated by subtracting the changes recorded for the biosensor when it was loaded with mAb/MHC/TCR in the absence of biotinylated SEB.

Competitive Binding Assay—All competitive binding with TCR, MHC, and the mAbs toward SEB were conducted in binding buffer (1× PBS supplemented with 1% BSA) to limit nonspecific binding to the biosensor. TCR protein was kindly provided by Prof. Luc Teyton (Scripps Research Institute), and the monomer MHC protein was provided by National Institutes of Health tetramer core facility. A typical binding experiment involved prewash, loading, and baseline, as described above. Also an additional loading step was introduced that immobilized various concentrations of mAbs (20B1, 14G8, or 6D3) onto the biotinylated SEB biosensor. The biosensor tip was then incubated with the binding buffer for 30 s to remove all unbound antibodies. This was followed by the association step where either 164 μM of TCR or 3.2 μM of MHC was incubated with the immobilized SEB·mAb complex for 90 s. All nonspecific binding to the biosensor was eliminated by subtracting the changes recorded for the biosensor when loaded with antibody and TCR (or MHC) in the absence of biotinylated SEB.

Sequential Binding of mAbs—Steps involved in the sequential binding of all three mAbs was similar to that used for direct binding study assay (see above), except that two additional loading and wash steps were introduced. Proper controls were run to test whether mAbs were dissociating from SEB immobilized onto the biosensor. There was no decrease in the capture level, even when the dissociation step was extended beyond 500 s. All data analysis was done using the ForteBio software.

SEB-Fab Complex Crystallization—Complexes of SEB with bound Fabs were prepared as described above and crystallized by sitting drop vapor diffusion, mixing 0.2 μl of protein stock with 0.2 μl of well solution. Well solution conditions for the SEB·$20B1_{Fab}$ crystals were 0.1 M Na-HEPES, pH 7.5, 20% (w/v) PEG 6000. Well solution conditions for the SEB·$14G8_{Fab}$ crystals were 80 mM sodium cacodylate, pH 6.5, 16% (w/v) PEG 8000, 160 mM $Mg(CH_3COO)_2$, 20% (v/v) glycerol. Well solution conditions for the SEB·$14G8_{Fab}$·$6D3_{Fab}$ crystals were 0.1 M phosphate-citrate buffer, pH 4.2, 6.7% (w/v) PEG 3000, 0.5 M NaCl.

SEB-Fab Crystal Structure Determination—Data collection on SEB·Fab crystals was done at Beamlines X4 and X29 of the National Synchrotron Light Source (see Table 1 for details). The first structure solved (SEB·$20B1_{Fab}$) was solved by molecular replacement using Phaser (23), with free SEB (PDB code 1SE4) and a Fab structure with high sequence identity (PDB code 1JHK) as search models. The crystallographic *R* factor with all models placed was 0.45; the *Z* score of the final translation search was 35. The SEB·$14G8_{Fab}$ structure was solved similarly, using PDB codes 1SE4, 3FFD, and 3D9A as search models for the SEB, $14G8_{Fab}$ heavy chain, and $14G8_{Fab}$ light chain, respectively (*R* factor with all models placed, 0.46; *Z* score, 32). The SEB·$14G8_{Fab}$·$6D3_{Fab}$ structure was also solved by molecular replacement, using SEB and $14G8_{Fab}$ from the refined SEB·$14G8_{Fab}$ structure as search models for their parts of the complex, and PDB code 3GI8 as a search model for the 6D3 Fab (*R* factor with all models placed, 0.46; *Z* score, 27). All SEB·Fab structures were refined using Refmac and manually rebuilt using Coot (see Table 1 for refinement statistics).

NMR Data Collection: NMR Resonance Assignment—300 μM ^{13}C-^{15}N-labeled SEB in 20 mM Tris pH 7.5 buffer was used to collect the data for backbone resonance assignments. Details of the backbone resonance assignment will be published separately. Briefly, the following experiments were recorded ^{1}H-^{15}N HSQC (512 and 128 complex points with sweep widths of 13 and 35 ppm in ^{1}H and ^{15}N dimensions, respectively), HNCO (512, 32, and 50 complex points with sweep widths of 13, 35, and 12 ppm in ^{1}H, ^{15}N, and ^{13}C dimensions, respectively) and HNCACB/CBCACONH pair (512, 32, and 50 complex points with sweep widths of 13, 35, and 65 ppm in ^{1}H, ^{15}N, and ^{13}C dimensions, respectively) (24, 25) to obtain the backbone resonance assignments of SEB. All experiments were carried out at 25 °C using Bruker Avance (800 and 900 MHz) spectrometers equipped with 5-mm TCI cryogenic probes capable of applying pulse-field gradients along the *z* axis. NMR data were processed using NMRPipe (26) and analyzed using NMRViewJ (27).

NMR Titrations to Determine SEB-Fab Interactions—Spectral perturbations in ^{1}H-^{15}N HSQC spectra of 50 μM uniformly ^{15}N,^{2}H-labeled and ^{15}N-labeled SEB (in NMR buffer, described above) were obtained by separate titrations with unlabeled Fab fragments at concentrations of 12.5, 25, 37.5, 50, and 100 μM. In addition, TROSY (28)/CRINEPT (29) experiments were acquired for the SEB·Fab complex, which contained 50 μM ^{15}N,^{2}H-labeled SEB and 100 μM of unlabeled Fab fragments (20B1, 14G8, and 6D3). CRINEPT experiments were recorded

TABLE 1
Data collection and refinement statistics

	SEB·20B1	SEB·14G8·6D3	SEB·14G8
Data collection			
Space group	$P2_1$	C2	$P2_12_12_1$
Unit cell: *a*, *b*, *c* (Å)	56.5, 83.7, 174.7	301.3, 109.8, 82.8 ($\beta = 94.5$)	84.6, 85.3, 115.0
X-ray source	NSLS X4C	NSLS X29	NSLS X4C
Wavelength (Å)	0.979	1.075	0.979
Bragg spacings (Å)	100–2.7 (2.75–2.70)	100–2.7 (2.75–2.70)	100–1.8 (1.83–1.80)
No. of unique reflections	43,919 (2,077)	73,214 (3,657)	77,133 (3,451)
Multiplicity[a]	7.2 (4.9)	4.3 (3.8)	12.4 (4.6)
Average $(I)/(s_I)$[a]	16.1 (2.5)	19.9 (1.8)	38.5 (1.8)
Completeness (%)[a]	99.7 (95.8)	98.9 (98.2)	99.3 (89.9)
R_{merge} (%)[a,b]	15.8 (50.3)	9.4 (74.1)	8.2 (56.1)
Refinement			
Resolution (Å)	2.7	2.7	1.8
R/R_{free} (%)[c,d]	22.5/27.6	24.0/27.8	14.2/18.9
Molecules in asymmetrical unit	2 SEB·20B1 complexes	2 SEB·14G8·6D3 complexes	1 SEB·14G8 complex
Total protein atoms	20,456	32,987	10,246
Bound ligands/ions	None	None	1 acetate
Total waters	147	None	908
RMSD bond length (Å)	0.007	0.015	0.013
RMSD bond angle (°)	1.06	1.45	1.40
Ramachandran favored/allowed (%)	94.8/99.3	92.8/98.8	97.0/99.7
PDB code	4RGM	4RGN	4RGO

[a] Values for the outermost shell are given in parentheses.
[b] $R_{merge} = (\sum|I_i - <I_i>|)/\sum|I_i|$, where I_i is the integrated intensity of a given reflection.
[c] $R = \sum||F_o| - |F_c||/\sum|F_o|$, where F_o and F_c denote observed and calculated structure factors, respectively.
[d] R_{free} was calculated using a random 5% of data excluded from refinement.

with the transfer time of 3.3 ms with 512 and 128 complex points in the ^1H and ^{15}N dimensions, respectively. All titration experiments were done at 25 °C on a Bruker Avance 900 spectrometer equipped with 5-mm TCI cryogenically cooled probes with a recycle delay of 1 s.

RESULTS

Combination of mAb 14G8 with mAb 20B1 or mAb 6D3 Enhances Efficacy of SEB Neutralization—First, we demonstrated that, *in vitro*, the combination of SEB specific mAb 14G8 with mAb 6D3 was more potent in inhibiting T-cell proliferation than either mAb alone at the same concentration (Fig. 1*A*). In contrast, the combination of mAb 20B1 with nonprotective mAb 14G8 did not result in enhanced inhibition of T-cell proliferation compared with mAb 20B1 alone. Next, *in vivo* SEBILS experiments confirmed that protective efficacy of mAb 6D3 was enhanced significantly by combining with mAb 14G8 (Fig. 1*B*). When used alone, mAb 14G8 exhibits no protective efficacy *in vivo*, even at the highest doses (500 μg) administered. *In vitro* assays (see above) did not demonstrate enhancement of mAb 20B1 efficacy through combination with mAb 14G8; however, *in vivo* experiments in mice did suggest that for this mAb as well protective efficacy was potentiated by combination therapy. Specifically, at low doses (50 μg) mAb 20B1 protected more mice against SEBILS if co-administered with a low dose mAb 14G8 (Fig. 1*B*). Taken together, these experiments support further investigations exploring the mechanism of combination therapy.

SEB Binding by mAbs—BLI assays determined the binding affinities for SEB of mAb 20B1, mAb 14G8 and mAb 6D3 to be 22.9 ± 7.4, 7.9 ± 1.5, and 11.8 ± 4.1 nM, respectively (data not shown). There was a very slight decrease in the response signal during the dissociation step of the assay (up to 500 s), an observation indicating a slow off rate consistent with the nanomolar binding constants of all three mAbs to SEB. The *in vitro* and *in vivo* protective assays indicated that more than one mAb could interact with SEB simultaneously (17). Therefore, simultaneous and sequential binding of two or more mAbs to SEB was investigated using BLI. When tested sequentially, an increase in the BLI response signal with each addition of any of the three mAbs is observed, consistent with the hypothesis that each mAb can bind to SEB independently (Fig. 2*A*). Furthermore, the binding was independent of the order of mAb addition; any combination of mAbs could sequentially bind to SEB (data not shown). A similar result was observed for a simultaneous binding assay: when two mAbs were present simultaneously at 50 nM each, the BLI response was higher than when a single mAb was present at 100 nM (Fig. 2*B*). Although the total amount of protein used was the same when mAbs were tested in pairs or alone, the higher BLI response signal when both mAbs were present indicates simultaneous binding to SEB. These data confirm ELISA-based predictions of nonoverlapping epitopes, which permit simultaneous binding of all three mAbs to SEB (17).

SEB Clearance Enhanced by Combination Therapy—Simultaneous binding of multiple mAbs to SEB is expected to result in an immune complex that can cross-link Fc receptors (FcRs) and promote cellular uptake. Consequently, we investigated clearance of SEB from serum in the setting of combination therapy. Enhanced clearance from serum was observed by ELISA in those mice injected with SEB and treated with the combination of mAb 14G8 and mAb 20B1 (Fig. 3*A*), but not in those mice that were treated with a mixture of mAb 14G8 and mAb 6D3 (Fig. 3*B*). To test whether FcR cross-linking promoted rapid internalization and clearance of SEB, we compared SEB uptake by primary peritoneal macrophages from FcR-deficient mice ($FcR\gamma^{-/-}$/$RIIB^{-/-}$) to uptake by the respective WT mice in the presence of one or two SEB specific mAbs. These experiments demonstrated enhanced SEB uptake by WT macrophages when mAb 20B1 and mAb 14G8 were combined, which was

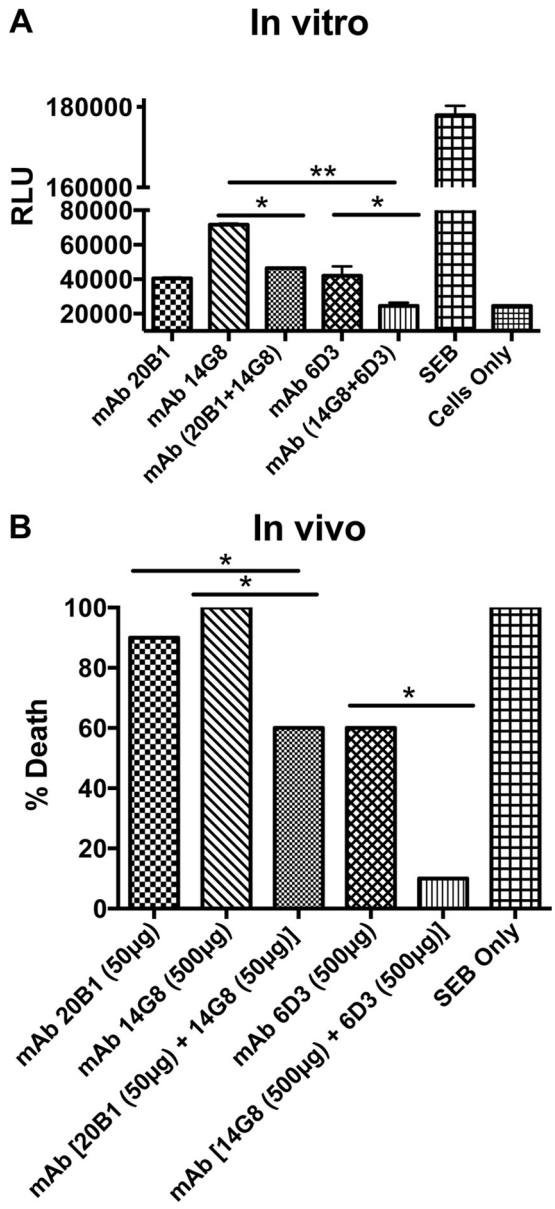

FIGURE 1. **Combination efficacy enhances SEB neutralization *in vitro* and *in vivo*.** *A*, inhibition of T-cell proliferation by SEB-specific mAbs 20B1, 14G8, and 6D3, individually at concentration of 5 μg or in different combinations of 2.5 μg each followed by SEB (25 nM). Proliferation was measured by ViaLight HS cell proliferation kit after 96 h. *B*, protection against SEBILS was tested in BALB/c mice ($n = 10$ per group) that were injected intraperitoneally with 20 μg of SEB and treated with mAb alone or in combination. Analysis of survival data was performed using Mantel-Cox Test. Mice treated with combination of mAbs 6D3 (500 μg) and 14G8 (500 μg) or 20B1 (50 μg) and 14G8 (50 μg) significantly survived, although monotherapy with the individual mAb was either non-protective (mAb 14G8 at 500-μg dose and mAb 20B1 at 50-μg dose) or partially protective (mAb 6D3 at 500-μg dose). *, $p < 0.05$; **, $p < 0.01$.

lost when FcR$\gamma^{-/-}$/RIIB$^{-/-}$ macrophages were used (Fig. 3*C*). However, consistent with serum clearance data (Fig. 3*B*), enhanced SEB uptake was not induced when mice were treated with mixture that included mAb 14G8 and mAb 6D3 (Fig. 3*D*). Similar results were observed when SEB internalization by neutrophils was compared between those treated with combination or mAb alone (Fig. 3, *E* and *F*). Again, significant enhancement in SEB uptake was achieved only when the first mixture was used (mAbs 14G8 with mAb 20B1) but not the second mixture (mAb 14G8 with mAb 6D3). Taken together, these data indicate that clearance through FcR-mediated uptake contributes to the enhanced neutralization efficacy observed in mice treated with a combination of mAb 20B1 and mAb 14G8. This mechanism does not explain the enhanced efficacy of combination therapy seen with mAb 6D3 and mAb 14G8 (Fig. 1*B*). Consequently, in-depth characterization of epitope bound by the mAbs was pursued.

SEB Specific mAbs Recognize Distinct Conformational Epitopes—X-ray crystal structures of SEB with Fab fragments were determined as binary (SEB·20B1$_{Fab}$ and SEB·14G8$_{Fab}$) and ternary (SEB·14G8$_{Fab}$·6D3$_{Fab}$) complexes. The Fab fragments of 20B1$_{Fab}$, 14G8$_{Fab}$ and 6D3$_{Fab}$ described in this study each have a typical Ig fold consisting of the light (V_L and C_L) and heavy (V_H and C_H) chains. Each of the four domains has one intrachain disulfide bond, typically seen in Ig Fab fragments. The ribbon structures of the binary SEB·20B1$_{Fab}$ complex and the ternary complex of SEB·14G8$_{Fab}$·6D3$_{Fab}$ are shown in Fig. 4 (*A* and *B*), respectively, colored as SEB (*blue*), 20B1$_{Fab}$ (*gold*), 14G8$_{Fab}$ (*green*), and 6D3$_{Fab}$ (*magenta*). The SEB residues that interact with Fab fragments are colored on the surface plot of SEB (Fig. 4, *C* and *D*). These data reveal that each of the Fabs binds to a distinct conformational epitope on the surface of SEB. Although all three binding surfaces are located on one side of SEB (Fig. 4*D*), there is no overlap of the epitope defining residues that would occlude the binding of another mAb, which is consistent with the BLI data (Fig. 2).

SEB·20B1$_{Fab}$ Binary Complex—A superposition of the apo-SEB (PDB code 3SEB) (30) structure (*blue*) with the SEB molecule of the SEB·20B1$_{Fab}$ (PDB code 4RGM) complex (*gold*) gives a root mean square difference (r.m.s.d.) of 0.53 Å calculated for all the backbone atoms (Fig. 5*A*). The complex is formed through the contacts between the residues from the CDR1 (Tyr^{32}) and CDR2 (Tyr^{91}, Ala^{92}, Tyr^{94}, and Trp^{96}) regions of the light chain and the CDR1 (Thr^{30}), CDR2 (Asn^{52}, Thr^{53}, His^{54}, Gly^{56}, Ser^{55}, and Val^{57}), and CDR3 (Tyr^{101}, Gly^{102}, Asn^{104}, and Val^{107}) regions of the heavy chain. There are two other residues (Trp^{50} and Thr^{74}) of the heavy chain, which fall outside the CDR region but are involved in the binding with SEB. The conformational epitope on the surface of SEB that is recognized by 20B1$_{Fab}$ is formed by the cluster of residues: Thr^{18}, Gly^{19}, Leu^{20}, Glu^{22}, Asn^{23}, Val^{26}, Asp^{29}, Asp^{30}, Asn^{31}, Leu^{58}, Gly^{59}, Asn^{60}, Asn^{88}, Tyr^{90}, Arg^{110}, Phe^{177}, and Asn^{178} (Table 2). The total solvent-accessible surface areas of SEB and 20B1$_{Fab}$ buried after forming the complex are 932 and 929 Å^2, respectively, of which the light and heavy chain contribute 18 and 82%, respectively. There is no major conformational change in the structure of SEB upon binding, but side chain rearrangements were observed (Fig. 5*B*). The nanomolar affinity of SEB with mAb 20B1 ($K_d = 22.9 \pm 7.4$ nM) can be attributed to a network of intermolecular hydrogen bonds and several hydrophobic-hydrophobic interactions between SEB and 20B1$_{Fab}$ residues. The hydrogen bonds are formed primarily through the side chain rearrangements of the SEB and 20B1$_{Fab}$ residues: Thr^{18}–Asn^{104}, Leu^{20}–Asn^{104}, Glu^{22}–Asn^{52}, Asn^{23}–Tyr^{101}, Leu^{58}–Thr^{74}, Gly^{59}–Thr^{74}, Asn^{60}–Thr^{53}, Asn^{88}–His^{54}, Arg^{110}–Thr^{74}, and Asn^{178}–Tyr^{91} where the first residue is from SEB and the second one is from 20B1 (Table 2). Some of the stability seen in

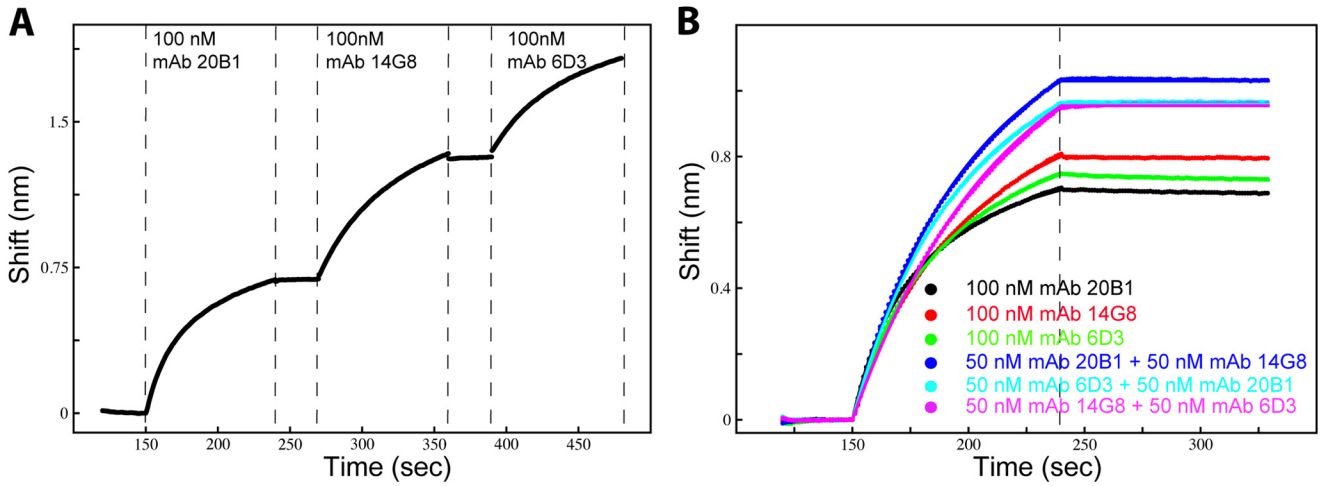

FIGURE 2. **Binding studies of SEB with mAbs.** *A*, BLI assay showing the sequential binding of the mAbs 20B1, 14G8, and 6D3 (100 nM) to SEB immobilized on the biosensor tip. The *vertical dashed lines* indicate when each individual antibody is being incubated with SEB. *B*, comparing the binding response of mAbs when incubated with SEB singly or in combination. The binding responses of 100 nM mAb 20B1 (*black*), mAb 14G8 (*red*), and mAb 6D3 (*green*) are compared with binding response obtained when combination of mAbs were used: mAb 20B1 and mAb 14G8 (*blue*), mAb 20B1 and mAb 6D3 (*cyan*), and mAb 14G and mAb 6D3 (*magenta*). Each combination mixture had 50 nM of individual mAbs making the final concentration of 100 nM. The *vertical dashed line* indicates when mAbs were removed from flow through.

the SEB·20B1$_{Fab}$ complex is also contributed to the hydrophobic interactions seen between the residues Leu^{20} and Phe^{177} of SEB with residues Tyr^{101}, Val^{107}, Trp^{50}, Tyr^{91}, Tyr^{94}, and Trp^{96} of 20B1, respectively (Fig. 6*A*, *right panel*). The side chain of residue His^{54} of the heavy chain fits into the hydrophobic pocket formed by residues Val^{26}, Asn^{88}, and Tyr^{90} of SEB (Fig. 6*A*, *left panel*).

SEB·14G8$_{Fab}$ Binary Complex—The apo structure of the SEB (PDB code 3SEB) shown in blue ribbon plot in Fig. 5*C* is superimposed with the SEB molecule of the SEB·14G8$_{Fab}$ (PDB code 4RGO) complex (*green*). The r.m.s.d. between the backbone atoms of apo SEB and SEB molecules in the SEB·14G8$_{Fab}$ complex is ~0.62 Å, which also suggests that there is no major conformational change seen in the SEB molecule upon interacting with 14G8$_{Fab}$. However, several side chain reorganizations were seen in the SEB residues involved in direct binding (Fig. 5*D*). The conformational epitope on the surface of SEB that is recognized by 14G8$_{Fab}$ is formed by the cluster of the following residues: Asp^{5}, Pro^{6}, Pro^{8}, Arg^{135}, Phe^{137}, Asp^{139}, Gly^{140}, Lys^{141}, Asn^{142}, Ser^{145}, Tyr^{186}, Lys^{188}, Ile^{190}, Lys^{229}, Glu^{231}, Tyr^{233}, and Thr^{235}. For the antibody, all the residues involved in forming the complex with SEB belong to CDR1 (Asp^{31} and Tyr^{32}), CDR2 (Tyr^{50} and Gln^{53}), and CDR3 (His^{92} and Phe^{94}) of the light chain and CDR1 (Thr^{28}, Ser^{30}, Ala^{31}, and Tyr^{32}), CDR2 (Ser^{52}, Ser^{56}, and Tyr^{58}), and CDR3 (Tyr^{100}, Gly^{101}, Asp^{102}, Tyr^{103}, Val^{104}, and Arg^{106}) of the heavy chain (Table 2). The total solvent-accessible surface areas of SEB and 14G8$_{Fab}$ buried in the complex are 941 and 928 Å^2, respectively, of which the light and heavy chain contributed 36 and 64%, respectively. The nanomolar binding affinity (7.9 ± 1.5 nM) measured for the SEB·14G8 complex can be attributed to the vast network of intermolecular hydrogen bonds and electrostatic interactions such as salt bridges (Arg^{135}–Asp^{31} and Glu^{231}–Arg^{106}) being formed between residues of SEB and 14G8$_{Fab}$. Except for one hydrogen bond that is formed between the backbone amide and carbonyl oxygen (Gly^{140}–Val^{104}), the remaining hydrogen bonds are formed primarily through side chain rearrangements of the following SEB and 14G8$_{Fab}$ residues: Asp^{5}–Tyr^{32}, Arg^{135}–Asp^{31}, Arg^{135}–Tyr^{32}, Asn^{142}–His^{92}, Tyr^{186}–Ala^{31}, Lys^{188}–Tyr^{100}, Glu^{231}–Arg^{106}, and Glu^{231}–Tyr^{50}, where the first residue belongs to SEB, and the second residue belongs to antibody.

SEB·14G8$_{Fab}$·6D3$_{Fab}$ Ternary Complex—To investigate whether the same lack of conformational change would be true when two Fab fragments were bound to SEB simultaneously and to define the epitope of mAb 6D3, we solved the ternary complex structure formed between SEB bound to 14G8 and 6D3 Fab fragments (PDB code 4RGN). The overall r.m.s.d. between the common backbone atoms of SEB and 14G8$_{Fab}$ in the binary (SEB·14G8$_{Fab}$) and ternary (SEB·14G8$_{Fab}$·6D3$_{Fab}$) complexes is 0.99 Å. The r.m.s.d. between the backbone atoms of apo SEB (PDB code 3SEB) and SEB molecule in the ternary complex is 0.67 Å (Fig. 5*E*), again suggesting that there are no major conformational changes induced in the SEB molecule when two Fab fragments (14G8 and 6D3) bind. The residues involved in the binding region of SEB and 14G8$_{Fab}$ are identical to the binary complex and therefore are not reported again. The conformational binding epitope of 6D3$_{Fab}$ on SEB involves residues Gly^{123}, Gln^{125}, Leu^{126}, Asp^{127}, Lys^{128}, Tyr^{129}, Arg^{130}, Ser^{131}, Asn^{149}, Lys^{153}, and Lys^{226}, which corresponds to 835 Å^2 solvent-accessible area buried upon complex formation. The light and heavy chain contribute 43 and 57% of the buried surface area, respectively. Because no major conformational changes are seen in the SEB molecule in SEB·14G8$_{Fab}$·6D3$_{Fab}$ complex, most of the interactions between SEB and 6D3$_{Fab}$ molecules are through the rearrangement of the side chains (Fig. 5*F*). The SEB·6D3$_{Fab}$ complex is formed through the contacts between the residues from the CDR1 (Gln^{27}, Asn^{31}) and CDR3 (Asp^{97}, Tyr^{98}, Thr^{99}, Tyr^{100}, and Leu^{102}) regions of the light chain and the CDR1 (Trp^{33}), the CDR2 (Asp^{52}, Asp^{55}, Tyr^{57}, and Ile^{58}) and the CDR3 (Thr^{99}, Leu^{102}, Leu^{103}, and Ala^{104}) regions of the heavy chain (Table 2). Similar to SEB·20B1$_{Fab}$ complex there are four residues (His^{35}, Glu^{50}, Tyr^{57}, and Asn^{59}) of the heavy chain, which fall outside the CDR

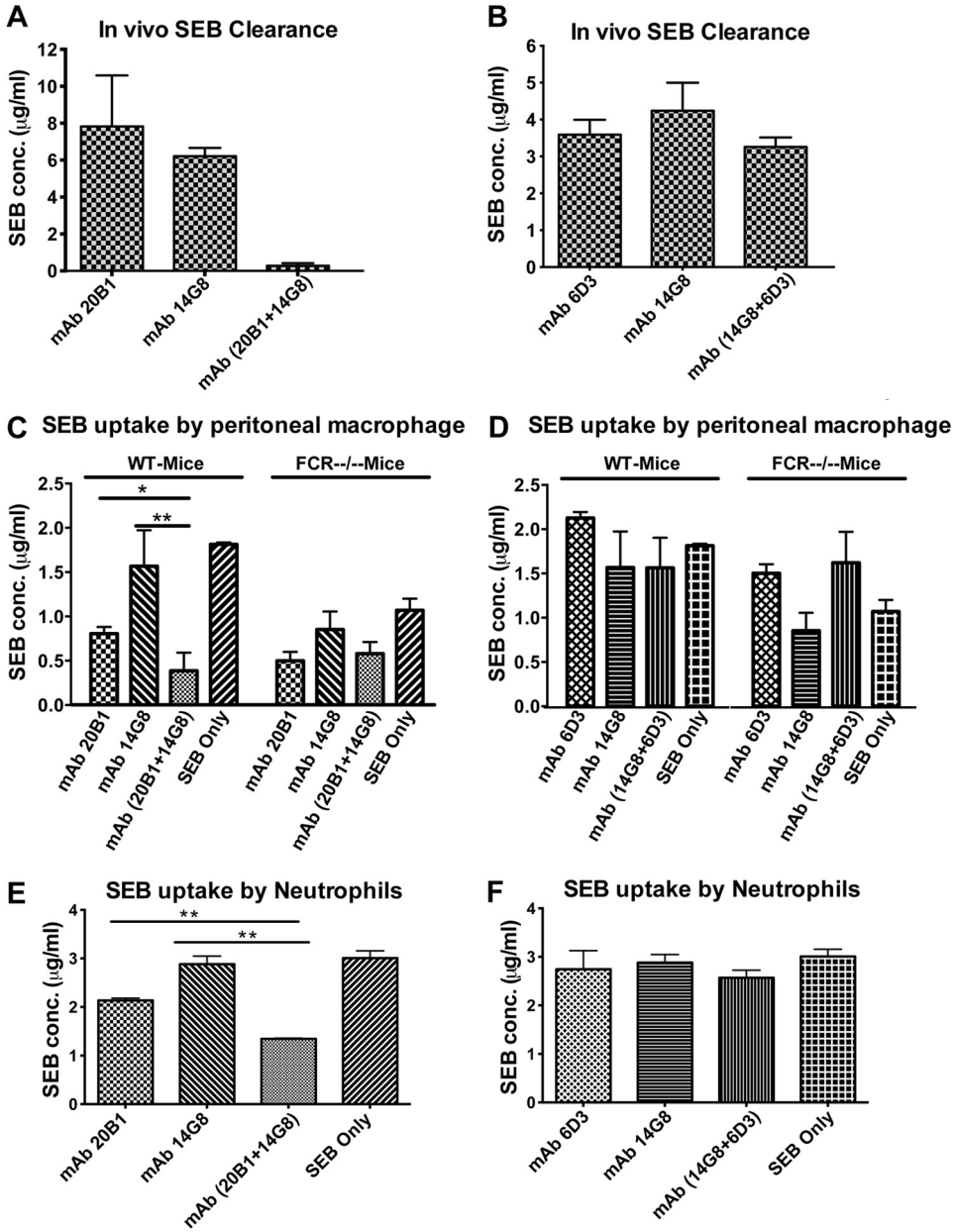

FIGURE 3. **Combination efficacy enhances clearance of SEB from body fluid.** *A* and *B*, mice ($n = 5$) were treated with mAb 20B1, mAb 14G8, and mAb 6D3 alone or in combination (500 μg) and challenged with SEB. ELISAs were performed to measure the SEB levels from sera at 6 h after SEB challenge. SEB level was higher in blood at 6 h in mice treated with mAb alone or in combination of mAb 14G8 and mAb 6D3. Higher SEB clearance was observed from sera of mice treated with combination of mAb 20B1 and mAb 14G8 group. *Error bars* represent the standard error derived from the SEB measurement of a group of five mice in each data set. *C* and *D*, SEB internalization with mAbs 20B1, 14G8, and 6D3 alone or in combination by primary peritoneal macrophage was performed in FcR ($FcR\gamma^{-/-}$/$RIIB^{-/-}$) knockout mice and compared with WT C57/BL6 mice. *E* and *F*, SEB internalization with mAb 20B1, mAb 14G8, or mAb 6D3 alone or in combination by purified human neutrophils. The *y* axis shows residual SEB concentration from the supernatant. *Error bars* represent the standard error derived from triplicate of independent experiments. *conc.*, concentration. *, $p < 0.05$; **, $p < 0.01$.

region but are involved in the binding with SEB. The total solvent-accessible surface area of $6D3_{Fab}$ covered by SEB is 833 Å^2. The nanomolar binding affinity observed for SEB·mAb 6D3 complex (11.8 ± 4.1 nM) is attributed to the formation of several intermolecular hydrogen bonds between the side chain (Asp^{127}–His^{35}, Asp^{127}–Thr^{99}, Asp^{127}–Tyr^{100}, Lys^{128}, Tyr^{100}, Lys^{128}–Ala^{104}, Arg^{130}–Tyr^{57}, Lys^{153}–Asp^{52} and Lys^{153}–Asp^{55}) and backbone (Asp^{127}–Leu^{103}, Tyr^{129}–Tyr^{98}, and Tyr^{129}–Tyr^{100}) atoms of the SEB and $6D3_{Fab}$. Furthermore, the stability of the SEB·6D3 complex is strengthened by the formation of two salt bridges between residues Lys^{128}–Asp^{97} and Lys^{153}–Asp^{52} of SEB and 6D3 molecule. The positively charged side chain of K128 is inserted inside the groove formed by the light and heavy chain residues of 6D3 and is stabilized by the formation of salt bridge with the negatively charged Asp^{97} of the light chain (Fig. 6*C*). Similarly the side chain of residue Asp^{127} is also buried inside the pocket and is stabilized by the formation of hydrogen bond with residues His^{35}, Thr^{99}, and Tyr^{100} of heavy and light chain (Table 2).

Comparison with SEB·Receptor Structures—The structures of the SEB·Fab complexes were superimposed with the previously published structures of the SEB·TCR (PDB code 1SBB)

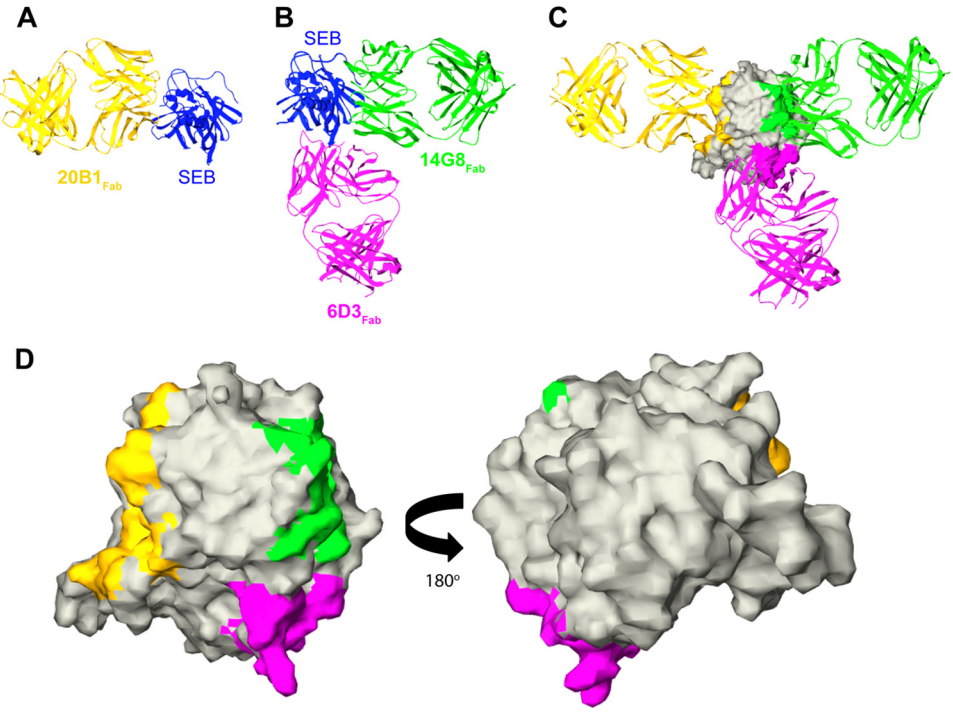

FIGURE 4. **Crystal structures of SEB in complex with Fabs 20B1, 14G8, and 6D3.** Ribbon and surface plots are color-coded as follows: SEB (*blue*), $20B1_{Fab}$ (*gold*), $14G8_{Fab}$ (*green*), and $6D3_{Fab}$ (*magenta*). *A*, binary complex of SEB and $20B1_{Fab}$. *B*, ternary complex of SEB with $14G8_{Fab}$ and $6D3_{Fab}$. *C*, composite overlay of the binary and ternary SEB complexes from *A* and *B*. SEB is shown as *gray surface*, and the residue interactions with Fabs are color-coded as described above. *D*, surface plot of apo-SEB (3SEB) shown in *gray* is colored with individual binding epitopes of $20B1_{Fab}$ (*gold*), $14G8_{Fab}$ (*green*), and $6D3_{Fab}$ (*magenta*).

(31) and SEB·MHC (PDB code 1SEB) (32) (Fig. 7). All the complex structures were aligned with the apo SEB (PDB code 3SEB) structure. For clarity the SEB molecule from complexes are not shown and all other structures are color-coded as follows: *gold* ($20B1_{Fab}$), *green* ($14G8_{Fab}$), magenta ($6D3_{Fab}$), *cyan* (MHC), and *red* (TCR). The binding site of $20B1_{Fab}$ completely overlaps with the binding site of TCR on SEB (Fig. 7*A*). There are 17 SEB residues that are in contact with the $20B1_{Fab}$ (see above and Table 2), and 11 (namely Thr^{18}, Gly^{19}, Leu^{20}, Glu^{22}, Asn^{23}, Asn^{60}, Tyr^{90}, Tyr^{91}, Phe^{177}, Asn^{178}, and Gln^{210}) of these 17 SEB residues also interact with the TCR (31). This steric occlusion of SEB to TCR by $20B1_{Fab}$ explains the high protective efficacy of mAb 20B1.

Although the binding sites of MHC on SEB do not overlap with those of $20B1_{Fab}$ (32), two SEB residues (Asn^{88} and Tyr^{90}) that interact with $20B1_{Fab}$ are close to the MHC binding SEB residues (Tyr^{89}, Asn^{92}, and Tyr^{94}), which may alter the binding of SEB to MHC. Importantly, the binding sites of $14G8_{Fab}$ and $6D3_{Fab}$ on SEB are distantly (>35 Å) located from both the TCR and the MHC binding sites (Fig. 7, *B* and *C*), consistent with their lack of potent neutralization when used alone despite being high affinity mAbs.

BLI Receptor Binding Assays—Structural results were validated by binding assays using BLI. Binding affinities of TCR (8.9 ± 3.0 μM) and MHC (4.06 ± 0.8 μM) with SEB were determined (data not shown), which are similar to those found in literature (33). Fig. 8*A* shows the variation in the response signal when TCR binds to SEB as a function of increasing concentration of mAb 20B1. The decrease in the response signal with increasing concentration of mAb 20B1 is expected, because the binding of TCR to SEB is occluded by mAb 20B1, as suggested by our structural studies (Fig. 7*A*). The percentage change in the binding of TCR to SEB in the presence of mAb 20B1, mAb 14G8, and mAb 6D3 as measured by BLI is shown in Fig. 8*D*.

Furthermore, the complex structures of SEB·$14G8_{Fab}$ and SEB·$6D3_{Fab}$ predicted that the binding of TCR would not be altered when either mAbs 14G8 or 6D3 is bound to SEB. However, our binding studies found that there was a ~34% decrease in binding of TCR when mAb 14G8 or mAb 6D3 was bound individually to SEB (Fig. 8, *B* and *D*). Similar binding assays were done with MHC in the presence of mAb 20B1, mAb 14G8, and mAb 6D3. In this case, we found that there was a ~37, ~41, and ~48% decrease in binding of MHC to SEB in the presence of mAb 20B1, mAb 14G8, and mAb 6D3, respectively (Fig. 8, *C* and *E*). Interestingly, when both mAb 14G8 and mAb 6D3 were bound to SEB, the binding of MHC to SEB decreased to ~66% (data not shown). The decrease in the binding of MHC to SEB in the presence of mAb 20B1 could be due to the slight conformational alteration in key binding residues as discussed above. However, decreased binding of MHC to SEB in the presence of mAb 14G8 and/or mAb 6D3 cannot be explained this way, because their binding sites are distant from the binding site of MHC. Therefore these results suggest that subtle conformational changes in SEB, which are not captured by the crystal structures, occur upon mAb binding in solution, thereby altering SEB binding of TCR and/or MHC.

NMR Spectral Analysis—NMR spectroscopy was used to further explore subtle changes that might occur at the TCR and MHC binding sites when mAbs/Fabs 14G8 and 6D3 are bound to SEB in solution. Backbone amide resonances (HN and N) are very sensitive to the changes in the molecular environment and thus act as excellent probes to study protein-protein, protein-

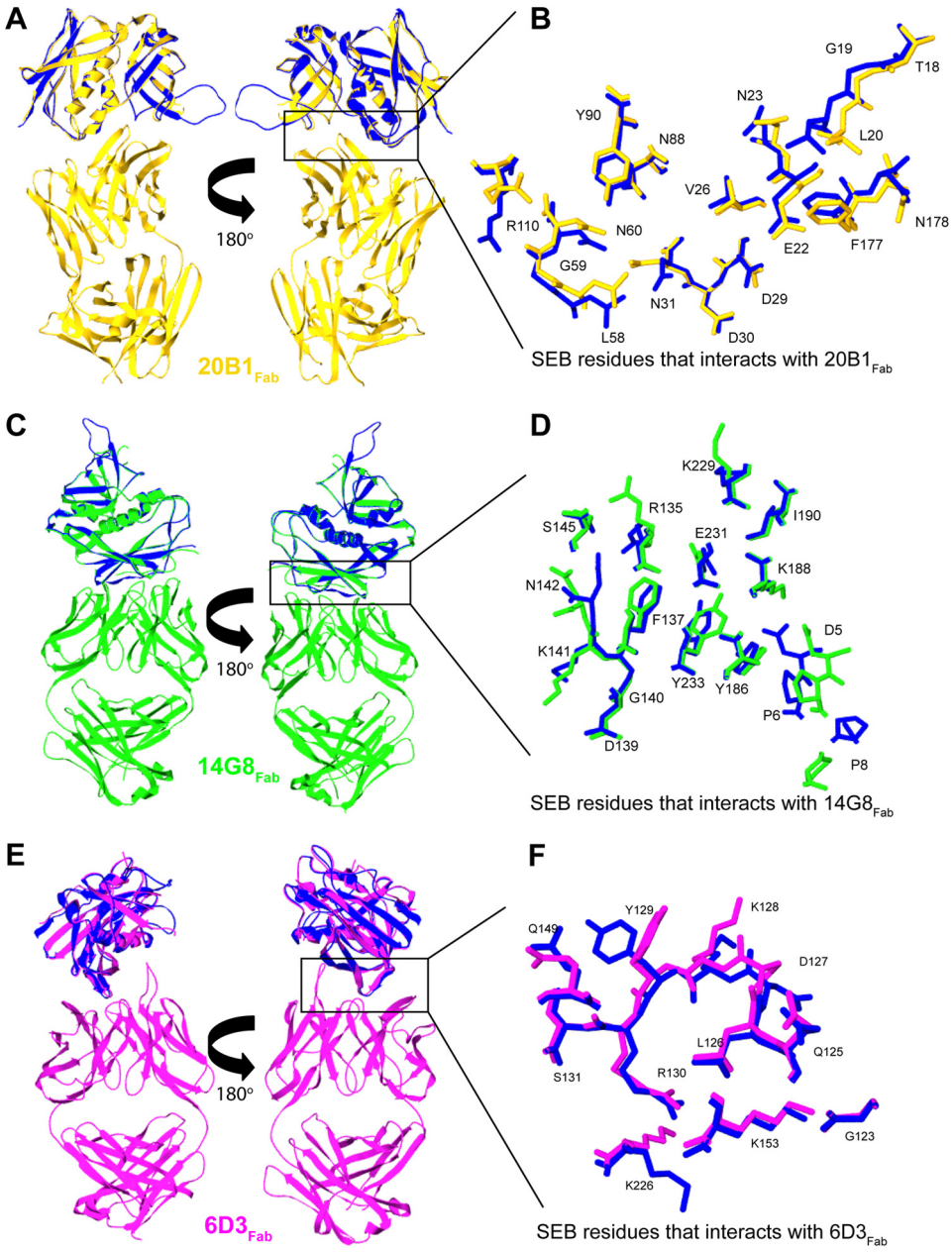

FIGURE 5. **Comparison of the crystal structure of apo-SEB with SEB in complex with Fabs.** All structures are shown as ribbon plot and are color-coded as follows: apo-SEB (*blue*), SEB·20B1$_{Fab}$ (*gold*), SEB·14G8$_{Fab}$ (*green*), and SEB·6D3$_{Fab}$ (*magenta*). Apo-SEB (3SEB) structure is superimposed with the SEB molecule of the binary complex SEB·20B1$_{Fab}$ (*A*), binary complex SEB·14G8$_{Fab}$ (*C*), and ternary complex SEB·14G8$_{Fab}$·6D3$_{Fab}$ (*E*). For clarity, the structure of 14G8$_{Fab}$ is not shown in *E*. *B*, *D*, and *F* show the side chain rearrangement (illustrated as ball and stick) of SEB residues upon binding with 20B1$_{Fab}$, 14G8$_{Fab}$, and 6D3$_{Fab}$, respectively. The color scheme is the same as described above.

ligand, or protein-nuclei acid interactions. Spectral changes of the backbone resonances, chemical shift perturbation, or peak attenuation can be monitored by recording a series of ^{1}H-^{15}N HSQC spectra of the protein with different amounts of ligand. Backbone resonances of SEB were assigned using standard triple resonance experiments. The interaction between SEB and Fabs (20B1, 14G8, and 6D3) results in a high molecular mass complex (~78 kDa) that requires the use of CRINEPT NMR experiments (26). CRINEPT is optimized for high molecular mass systems, and the majority of the backbone resonances corresponding to the complex are visible (data not shown). This experiment has been previously used to study a similar antibody-antigen interaction for the factor H binding protein (34). Mapping of SEB residues affected by the binding with Fab fragments was done by comparing spectral changes seen between the apo-spectrum (recorded as the TROSY-HSQC (28)) and the CRINEPT spectrum of the SEB·Fab complexes. If the resonance position in the CRINEPT spectrum is unchanged when compared with the apo-spectrum (TROSY), it is an indication that the chemical environment of that residue is unchanged in the SEB·Fab complex. Conversely, if a resonance is found to be missing in the CRINEPT spectrum, it indicates that the chemical environment of that resonance has been affected either because of direct binding interaction of the Fab fragments with SEB or because of structural rearrangement manifested as a result of complex formation. NMR titration data are presented

TABLE 2

SEB residues that interact with the residues from the light and heavy chain of the $20B1_{Fab}$, $14G8_{Fab}$, and $6D3_{Fab}$

Residues that are within 4 Å distance are listed below. Residues from CDR1, CDR2, and CDR3 regions are in underlined, italic, and bold text, respectively.

SEB residues	Residues		Hydrogen bond	Type of interaction
	Light chain	Heavy chain		
20B1				
Thr^{18}		**Asn^{104}**	Thr^{18}–Asn^{104}	
Gly^{19}		**Asn^{104}**		
Leu^{20}		**Asn^{104}, Tyr^{101}, Val^{107}**	Leu^{20}–Asn^{104}	Hydrophobic
Glu^{22}		Trp^{50}, *Asn^{52}*, **Tyr^{101}**	Glu^{22}–Asn^{52}	
Asn^{23}		**Tyr^{101}, Gly^{102}**	Asn^{23}–Tyr^{101}	
Val^{26}		*Asn^{52}*, *His^{54}*, *Ser^{55}*		
Asp^{29}		*Val^{57}*		
Asp^{30}		*Val^{57}*		
Asn^{31}		*Ser^{55}*		
Lsu^{58}		*Thr^{53}*, *Gly^{56}*, *Ser^{55}*, Thr^{74}	Leu^{58}–Thr^{74}	
Gly^{59}		Thr^{74}	Gly^{59}–Thr^{74}	
Asn^{60}		Thr^{30}, *Thr^{53}*, Thr^{74}	Asn^{60}–Thr^{53} Asn^{60}–Thr^{74}	
Asn^{88}		*His^{54}*	Asn^{88}–His^{54}	
Tyr^{90}		Thr^{30}, *His^{54}*		
Arg^{110}		Thr^{74}	Arg^{110}–Thr^{74}	
Phe^{177}	**Tyr^{91}, Tyr^{94}, Trp^{96}**			Hydrophobic
Asn^{178}	Tyr^{32}, **Tyr^{91}, Ala^{92}**		Asn^{178}–Tyr^{91}	
14G8				
Asp^{5}		Tyr^{32}	Asp^{5}–Tyr^{32}	
Pro^{6}		Thr^{28}, Ala^{31}		
Pro^{8}		Ser^{30}		
Arg^{135}	Asp^{31}, Tyr^{32}, *Tyr^{50}*		Arg^{135}–Asp^{31} Arg^{135}–Tyr^{32}	Electrostatic/salt bridge
Phe^{137}	*Tyr^{50}*	**Asp^{102}, Tyr^{103}**		
Asp^{139}		*Ser^{52}*, *Tyr^{58}*, *Ser^{56}*	Asp^{139}–Tyr^{58}	
Gly^{140}		*Ser^{52}*, **Asp^{102}, Tyr^{103}, Val^{104}**	Gly140–Val^{104a}	
Lys^{141}	**Phe^{94}**	*Tyr^{58}*		
Asn^{142}	Tyr^{32}, **His^{92}**		Asn^{142}–His^{92}	
Ser^{145}	Tyr^{32}			
Tyr^{186}		Ala^{31}	Tyr^{186}–Ala^{31}	
Lys^{188}		**Tyr^{100}**	Lys^{188}–Tyr^{100}	
Ile^{190}		**Tyr^{100}**		
Lys^{229}	*Gln^{53}*			
Glu^{231}	*Tyr^{50}*	**Tyr^{100}, Arg^{106}**	Glu^{231}–Arg^{106} Glu^{231}–Tyr^{50}	Electrostatic/salt bridge
Tyr^{233}		**Tyr^{100}, Gly^{101}, Asp^{102}**		
Thr^{235}		**Asp^{102}**		
6D3				
Gly^{123}		*Asp^{55}*		
Gln^{125}		Trp^{33}, **$Leu^{10}2$**		
Leu^{126}	**Tyr^{100}**	Tyr^{57}, Trp^{33}		Hydrophobic
Asp^{127}	**Tyr^{100}**	Trp^{33}, His^{35}, Glu^{50}, **Thr^{99}, Leu^{102}, Leu^{103}**	Asp^{127}–His^{35} Asp^{127}–Thr^{99} Asp^{127}–Leu^{103a} Asp^{127}–Tyr^{100}	Electrostatic/salt bridge
Lys^{128}	**Asp^{97}, Tyr^{98}, Tyr^{100}, Leu^{102}**	**Ala^{104}**	Lys^{128}–Asp^{97} K128–Tyr^{100} K128–Ala^{104}	
Tyr^{129}	Asn^{31}, **Tyr^{98}, Thr^{99}, Tyr^{100}**	**Leu^{103}**	Tyr^{129}–Tyr^{98a} Tyr^{129}–Tyr^{100a}	
Arg^{130}		Asn^{59}, *Tyr^{57}*	Arg^{130}–Tyr^{57} Arg^{130}–Asn^{59}	
Ser^{131}	**Thr^{99}**			
Gln^{149}	Gln^{27}, **Tyr^{98}**, **Thr^{99}**			
Lys^{153}		*Asp^{52}*, *Asp^{55}*, *Tyr^{57}*	Lys^{153}–Asp^{52} Lys^{153}–Asp^{55}	Electrostatic/salt bridge
Lys^{226}		*Tyr^{57}*, *Ile^{58}*		

[a] Backbone HN-CO.

as a heat map in which all residues perturbed upon Fab binding are colored *red* and unperturbed residues are colored *green* (Fig. 9).

As predicted from our crystal structures, the resonances of the SEB residues in contact with the $20B1_{Fab}$ (Fig. 9*A*, *first column*), $14G8_{Fab}$ (Fig. 9*B*, *second column*), and $6D3_{Fab}$ (Fig. 9*C*, *third column*) are missing in the CRINEPT spectra of the complex. Interestingly, the resonances belonging to SEB residues Asp^{29}, Asp^{30}, Tyr^{90}, and/or Asn^{178}, which are involved in binding with $20B1_{Fab}$, are also perturbed when $14G8_{Fab}$ or $6D3_{Fab}$ are bound to SEB. Similarly residue Lys^{229}, which directly contacts $14G8_{Fab}$, is perturbed when $20B1_{Fab}$ and $6D3_{Fab}$ are bound to SEB. It was expected that binding of TCR would be altered when $20B1_{Fab}$ is bound to SEB because both $20B1_{Fab}$ and TCR share the same binding epitope on SEB (Fig. 9*E*, *first column*). However, key residues (Leu^{20}, Glu^{22}, Tyr^{90}, and/or Asn^{178}) are also perturbed when $14G8_{Fab}$ and $6D3_{Fab}$ are bound to SEB (Fig. 9*E*, *second* and *third columns*). Similarly, residues involved in MHC binding are also perturbed when $20B1_{Fab}$, $14G8_{Fab}$, and $6D3_{Fab}$ are bound to SEB (Fig. 9*D*). Therefore, NMR results are consistent with data from competitive binding studies. We conclude that SEB binding of TCR and MHC can be altered in two ways: either by directly blocking interaction with key residues or through subtle conformational changes that are propagated within SEB when mAbs bind the toxin at distant sites.

Cross-protection of mAb 20B1 in Mice with SEC1-induced Lethal Shock—Next, a structural database of superantigens including SEC 1–3 and SSA was searched. This search identified residues that shared interaction of SEB with mAb 20B1. Superantigen SEC-1, which is 66% homologous to SEB, was found to have 14 of the 17 residues, involved in binding with $20B1_{Fab}$, to be identical (Fig. 10*A*). ELISA assays confirmed binding of mAb 20B1 to SEC-1 (Fig. 10*B*), and the binding affinity obtained from BLI analysis was 2.5 ± 0.45 nM. In contrast,

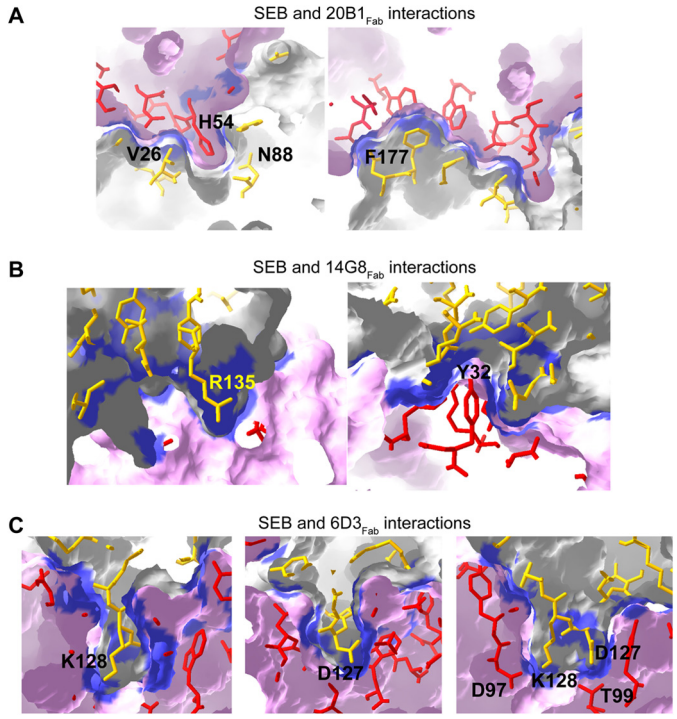

FIGURE 6. **The detail interactions at the interface of SEB·Fab complexes.** *A–C*, binding interface of SEB·20B1$_{Fab}$ (*A*), SEB·14G8$_{Fab}$ (*B*), and SEB·6D3$_{Fab}$ complexes (*C*). The SEB molecule is shown as *gray surface plot*, and the Fabs are shown as *magenta surface plot*. The interface is colored *blue*. The SEB and Fab residues involved in binding interactions are shown as *yellow* and *red* ball and stick, respectively.

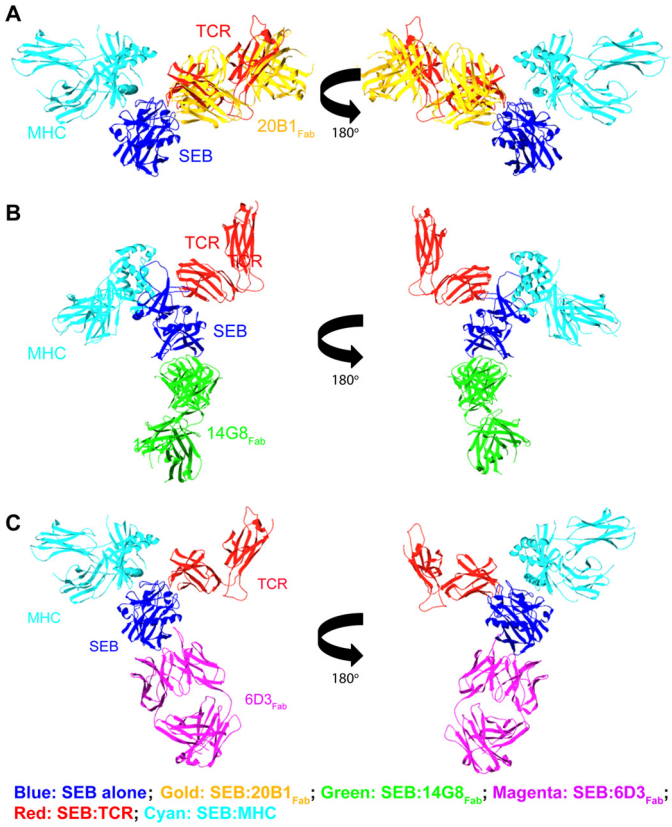

FIGURE 7. **Spatial positioning of Fabs, TCR, and MHC molecules around SEB.** All structures are shown as ribbon plot and color-coded as follows: apo-SEB (*blue*), SEB·20B1$_{Fab}$ (*gold*), SEB·14G8$_{Fab}$ (*green*), SEB·6D3$_{Fab}$ (*magenta*), SEB·TCR (*red*), and SEB·MHC (*cyan*). Superimposed structures of apo-SEB with the SEB molecule of SEB·20B1$_{Fab}$, SEB·TCR, and SEB·MHC (*A*); SEB·14G8$_{Fab}$, SEB·TCR, and SEB·MHC (*B*); and SEB·6D3$_{Fab}$, SEB·TCR, and SEB·MHC (*C*). For clarity, the SEB molecules from the complexes is not shown.

superantigen SEC-2 and SEC-3 did not bind mAb 20B1, although they share sequence homology but only have 11 of the 17 residues that interact with mAb 20B1. The same was true for streptococcal superantigen A (SSA), which also had 10 of the 17 interacting residues but failed to bind mAb 20B1 (Fig. 10*B*). Next, efficacy of mAb 20B1 to protect against SEC-1 intoxication in BALB/c mice was tested. Of 10 mice injected with SEC-1, 100% of mice treated with mAb 20B1 survived, whereas only 20% of untreated mice survived ($p < 0.0005$) (Fig. 10*C*).

DISCUSSION

SEB is one of the most potent superantigens known, with a low lethal dose and a rapid onset of symptomatic disease and death. As such, there has been a considerable amount of effort in the development of neutralizing mAbs against SEB as described elsewhere (17–20). The precise mechanisms by which these antibodies prevent SEB induced lethal shock are largely unknown because of the lack of precise epitope mapping. Antibodies developed in our lab have a range of protective efficacies (mAb 20B1 (high), mAb 6D3 (marginal), and mAb 14G8 (none) when administered alone. However, enhanced protective efficacies were documented when these mAbs were combined in cocktails (17) (Fig. 1). This observation of enhanced protective ability, when two mAbs are combined as a mixture, has also been described for other anti-SEB antibodies (18) without the knowledge of how enhanced protection is being achieved.

Historically, the affinity of mAbs was viewed as the single most important characteristic to predict neutralization efficacy. Because all three mAbs displayed similar nM binding affinities, and some only worked when combined, we pursued precise epitope mapping by x-ray crystallography. Binary (SEB·20B1$_{Fab}$ and SEB·14G8$_{Fab}$) and ternary complexes (SEB·14G8$_{Fab}$·6D3$_{Fab}$) readily provide an explanation for the highly protective nature of mAb 20B1 as compared with the other two mAbs. Our results clearly show that binding sites of TCR and mAb 20B1 are overlapping (Fig. 7*A*); therefore both mAb 20B1 and TCR will compete to bind SEB. Because the binding affinity of mAb 20B1 is ~1,000-fold greater than the binding affinity of TCR, the binding of SEB to TCR will be occluded, thus preventing the formation of the SEB·TCR·MHC trimer, the key step required for SEB to enact its superantigen function, which ultimately mediates its toxicity. The crystal structure of another SEB neutralizing mAb (3E2) shows that this mAb occludes the MHC binding site (35), and this suggests that the combination of mAbs 20B1 and 3E2 could potentially be synergistic. In contrast to mAb 20B1, both mAb 14G8 and mAb 6D3 binding epitopes are distinct but distant from the TCR or MHC epitopes on SEB (Fig. 7, *B* and *C*). This observation is consistent with the very low protective efficacies obtained for these two mAbs, when administered alone, because they would be unable to effectively prevent the productive formation of the SEB·TCR·MHC trimer. This inability to inhibit critical interactions of SEB with MHC or TCR explains

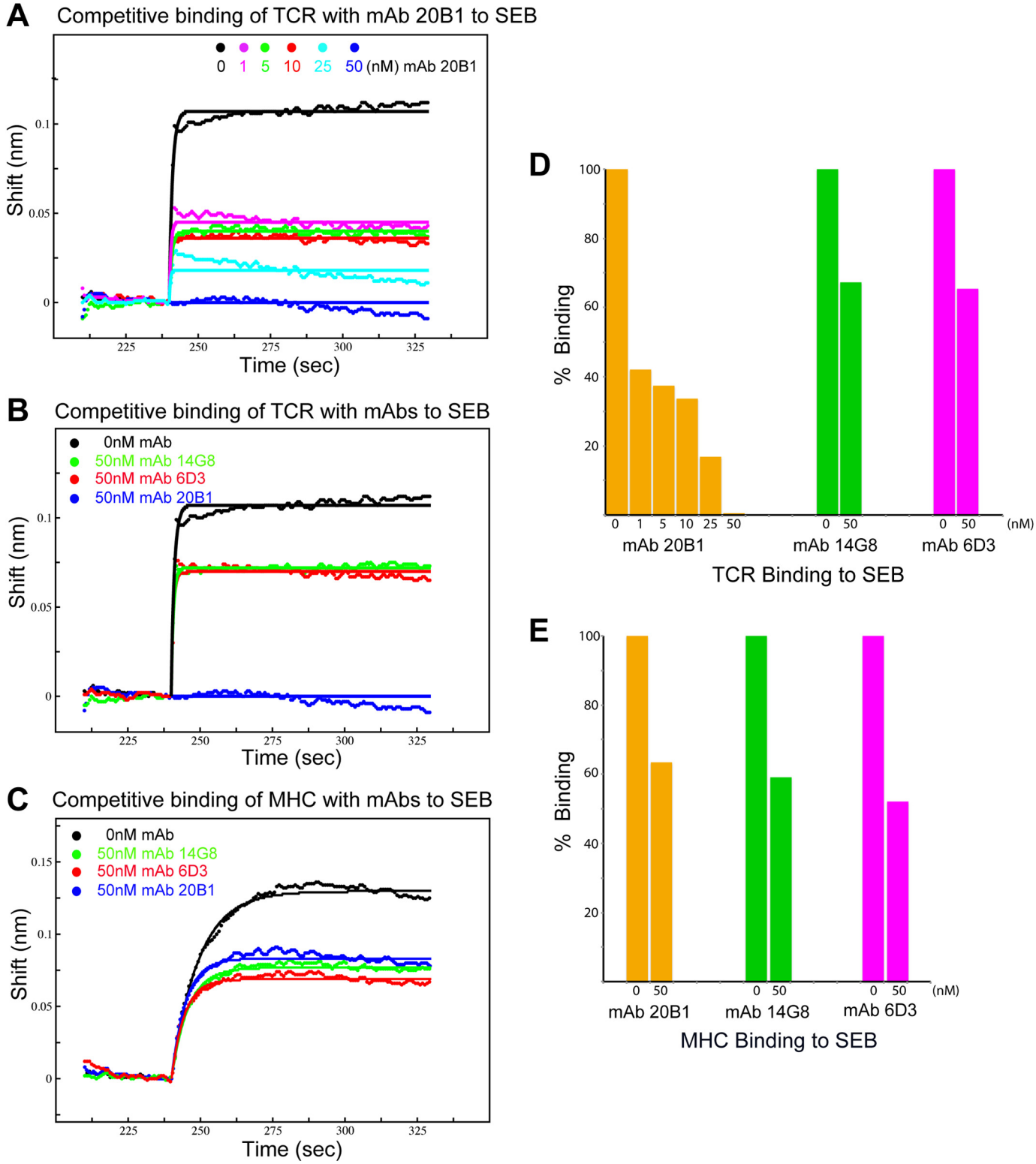

FIGURE 8. **TCR and MHC binding to SEB in presence of mAbs.** *A* and *B*, BLI response were measured for the binding of TCR (164 μM) to immobilized SEB in the presence of 0, 1, 5, 10, 25, and 50 nM mAb 20B1 (*A*) and 0 and 50 nM mAb 14G8 or 0 and 50 nM mAb 6D3 (*B*), respectively. *C*, similarly competitive binding studies of SEB with MHC (3.2 μM) in the presence of 0 and 50 nM mAb 20B1, mAb 14G8, and mAb 6D3, respectively, were done. All traces are colored as shown. *D* and *E*, the percentage binding of TCR (*D*) and MHC (*E*) were calculated from the competitive binding studies done in the presence of mAbs. The *bars* are color-coded as mAb 20B1 (*gold*), mAb 14G8 (*green*), and mAb 6D3 (*magenta*).

why mAb 14G8 and mAb 6D3 by itself is not protective against SEBILS, even at high concentrations (Fig. 3).

Direct binding to the TCR and MHC binding surface of the antigen by mAb, as observed for mAb 20B1 and mAb 3E2, is a well accepted mechanism of neutralization. However, there is mounting evidence that mAbs can exhibit more complex modes of action to achieve neutralization efficacy. First, several type II Abs exist for ricin and shiga toxin, which neutralize

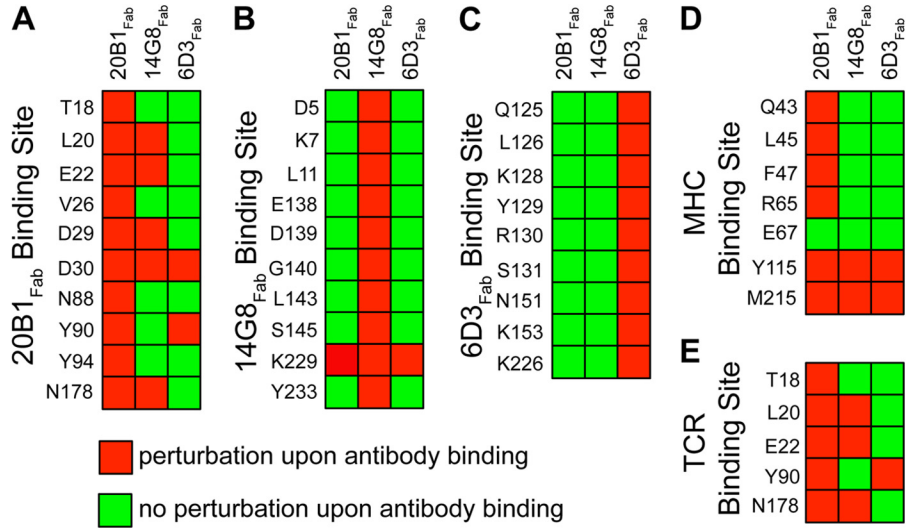

FIGURE 9. **NMR chemical shift perturbations upon binding of mAbs to SEB.** *A–E* show the chemical shift perturbation (as heat map) seen for the SEB residues that are involved in binding with $20B1_{Fab}$ (*A*), $14G8_{Fab}$ (*B*), $6D3_{Fab}$ (*C*), MHC (*D*), and TCR (*E*). The perturbations of the residues at each binding sites were compared when SEB was bound with $20B1_{Fab}$ (*first column*), $14G8_{Fab}$ (*second column*), and $6D3_{Fab}$ (*third column*). The residues that show perturbation from each binding sites are labeled. *Green* indicates that there was no change in the chemical shift for the indicated resonance in the CRINEPT spectra of SEB·$20B1_{Fab}$ (*first column*), SEB·$14G8_{Fab}$ (*second column*), and SEB·$6D3_{Fab}$ (*third column*) when compared with the apo-TROSY spectrum of SEB. *Red* indicates when the particular resonance is missing from the complex spectra when compared with the apo-SEB spectrum.

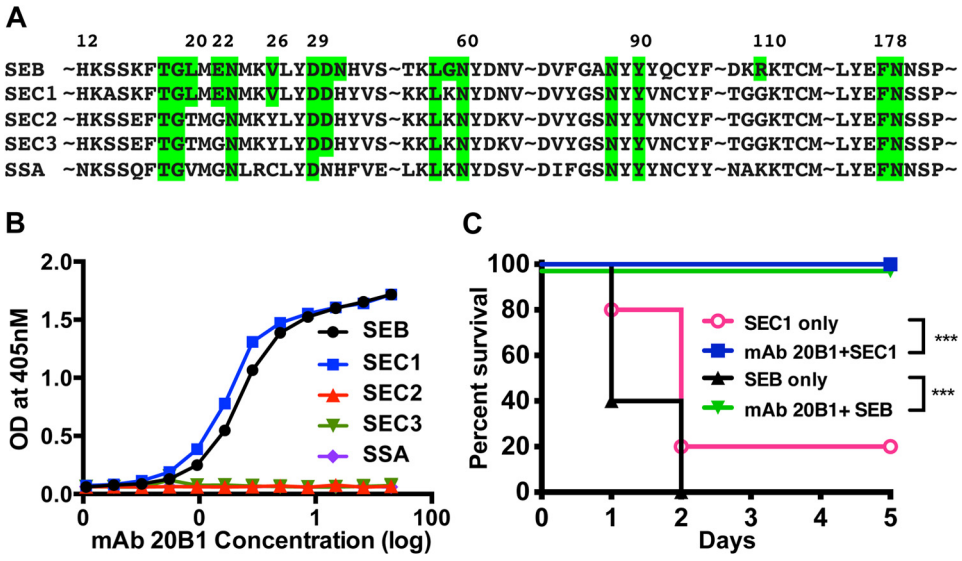

FIGURE 10. **Neutralization efficacy of mAb 20B1 on SEC-1 toxin.** *A*, sequence alignment of selected SEB residues to SEC1–3 and SSA. The 17 SEB residues involved in the binding with 20B1 are colored *green*. *B*, ELISA showing comparable binding of mAb 20B1 to SEB and SEC-1. mAb 20B1 failed to bind SEC 2–3 and SSA toxins. The experiment was performed in duplicate. Each point represents the mean value of duplicates, and *bars* represent the standard error derived from measurements in the same experiment. *C*, BALB/c mice ($n = 10$ per group) were treated with mAb 20B1 (500 μg) or PBS intraperitoneally (intraperitoneal) and challenged with 5 μg of SEB or SEC-1 and sensitized with 75 μg of LPS (intraperitoneal) 3 h post-toxin injection. Mice treated with mAb 20B1 showed 100% survival compared with PBS treatment. Analysis of survival data were performed using log rank (Mantel-Cox test). ***, $p < 0.001$.

intracellularly (36–38), *e.g.* through antibody-mediated inhibition of retrograde transport (39, 40). Second, a central role for the Fc fragment and host FcR have been demonstrated for neutralizing Abs of *B. anthracis* protective antigen (41), as well as SEB (42). Additionally, therapies using a combination of mAbs to achieve optimal protection have been described (8–13). Investigation of the potential for increased protective efficacies of our mAbs (20B1, 6D3, and 14G8) when administered as a mixture of two mAbs revealed that the presence of mAb 14G8 significantly enhanced the protective abilities of both mAb 20B1 and mAb 6D3 (Fig. 1).

Because neither mAb 6D3 nor mAb 14G8 directly inhibited the binding of either TCR or MHC to SEB, another mechanism must be responsible for the observed enhanced protections when mAb 14G8 was used in combination with mAb 20B1 or mAb 6D3. One possibility for this enhanced efficacy was accelerated clearance of the toxin through the FcR pathway. The therapeutic benefit of rapid clearance has been shown for botulinum toxin (43, 44) where mAbs binding to epitope tags decorate the toxin with multiple Fc domains, leading to accelerated FcR-mediated clearance. We confirmed that such a mechanism was activated when mAb 20B1 and mAb 14G8 were used in

combination, and thus accelerated clearance of SEB from mouse serum via an FcR-mediated pathway was documented (Fig. 3, *A* and *C*). However, our data also demonstrate that this did not occur when mAb 6D3 and mAb 14G8 were administered in combination (Fig. 3, *B* and *D*).

It is not clear why some combination therapies activate the FcR-mediated uptake by macrophages and some do not. We speculate that the angle at which mAbs bind leads to a specific conformation of immune complexes, which could facilitate cross-linking via the Fc subunits. However, in the case of combination treatment with mAbs 14G8 and 6D3, an alternate mechanism to explain the enhanced efficacy of this mixture is proposed, namely that antibody-induced allosteric changes in the SEB molecule subsequently reduce affinity of TCR and/or MHC binding to SEB. Although examination of the structures of SEB in various crystal forms (apo-SEB (PDB code 3SEB), SEB·$14G8_{Fab}$·$6D3_{Fab}$, SEB·TCR (PDB code 1SBB), and SEB·MHC (PDB code 1SEB)) revealed no major conformational rearrangements in the backbone structure of SEB in complex with the mAbs that would prevent TCR or MHC binding, there are subtle differences accounting for the small r.m.s.d. Additionally, side chain rearrangements can be observed at the SEB·Fab interfaces in our crystal structures (Fig. 5).

Allosteric changes upon mAb binding have been described for other mAbs (45). Specifically, conformation specific mAbs can allosterically augment the intrinsic activity of coagulation factor VIIa (46) and intrinsic factor X-activating complex (47), as well as the protease activity of protein D2 on the outer membrane of *Pseudomonas aeruginosa* (48). Binding studies of TCR with SEB in the presence of mAbs (20B1, 14G8, and 6D3) show that binding was reduced when mAb 20B1, mAb 14G8, and mAb 6D3 were bound to SEB. Similarly, the binding of MHC with SEB was also reduced when mAb 20B1, mAb 14G8, and mAb 6D3 were bound to SEB (Fig. 8). The complete loss of binding of TCR when mAb 20B1 is bound to SEB is expected, because both TCR and mAb 20B1 share the same binding site on SEB (Fig. 7*A*). However, the decrease in the binding of TCR and MHC when mAb 14G8 and mAb 6D3 is bound to SEB could be due to subtle structural changes induced upon antibody binding.

Further support stems from NMR spectroscopy of immune-complexes, which was used previously by Scarselli *et al.* (34) to determine the binding epitope of factor H binding protein of *Neisseria meningitidis* for which no crystal structure with the antibody was available. Importantly, CRINEPT NMR data (Fig. 9) confirmed the SEB residues involved in the direct binding with all three mAbs as identified in the binary and ternary complexes (Table 2). Notably, NMR data also revealed that the key interacting residues were similar to those identified by crystallography. However, the number of SEB residues affected by the interaction with each of the mAbs is larger than those observed in the crystal structure, indicating that the influence of mAb binding to SEB is propagated through the protein beyond the physical contacts. NMR is an ideal technique for investigating these subtle structural changes that may manifest in solution, because the resonance positions of individual amino acid residues are extremely sensitive to local environmental changes that can result from direct interactions or from allosteric rearrangements upon binding. Specifically, it can be seen that the resonances for Tyr^{115}, Met^{215}, Leu^{20}, Glu^{22}, Tyr^{90}, and Asn^{178}, all within the TCR and MHC binding sites of SEB, were also affected when SEB is bound to $14G8_{Fab}$ or $6D3_{Fab}$. The epitopes for mAb 14G8 and mAb 6D3 are remote from the TCR and MHC binding sites on SEB; therefore, these spectral changes result from subtle allosteric changes induced in SEB upon antibody binding. The combination of the NMR and BLI data support a novel mechanism of neutralization for mAb 14G8 and mAb 6D3 in combination that indirectly reduced binding, through allosteric changes, of SEB for the receptors. Additionally, we conclude that high *in vivo* efficacy of the mixture constituting of mAb 20B1 and mAb 14G8 is observed because three mechanisms are operative in the neutralization of SEB, the direct TCR inhibition by mAb 20B1, allosteric effect on SEB binding to MHC receptor by mAb 14G8, and enhanced clearance through FcR cross-linking by immune complex binding.

This study also highlights a second benefit of fine epitope mapping, namely the ability to predict cross-reactivity. Both SEB and SEC (SEC1–3) enterotoxins have ~66% identical protein sequence and have very similar structure (backbone r.m.s.d. ~0.75 Å). Our data identify 17 residues of SEB that bind $20B1_{Fab}$, which are conserved among SEBs derived from diverse clinical methicillin-sensitive and -resistant *Staphylococcus aureus* strains (49). Interestingly, of those 17 residues, 14 are identical in SEC1, and 11 are identical in SEC2 and SEC3, and 10 are identical in SSA. The latter is SSA, isolated from a *Streptococcus pyogenes* strain with known homology to SEB and SEC (50) that causes streptococcal toxic-shock-like syndrome. The fact that mAb 20B1 binds only to SEC1 and not to SEC2 or SEC3 indicates that three mAb 20B1 binding residues (Leu^{20}, Glu^{22}, and Val^{26}), which are not present in SEC2 and SEC3, may be important for the binding of SEB with mAb 20B1. Leu^{20} is probably less critical, because it can be changed to threonine (in SEC2 and SEC3) and valine (in SSA) with little structural interference. In contrast, substitution of Glu^{22} to glycine (in SEC2, SEC3, and SSA) results in the loss of a hydrogen bond to Asn^{52} of the 20B1 heavy chain, as well as loss of hydrophobic interactions with heavy chain residues Trp^{50} and Tyr^{101}. Substitution of Val^{26} with tyrosine (in SEC2 and SEC3) may cause substantial steric clashes with a number of 20B1 heavy chain residues, including Asn^{52}, His^{54}, Ser^{55}, and Tyr^{101} (Fig. 6*A*). It may be possible to re-engineer mAb 20B1 to produce a cross-reactive mAbs that could neutralize SEC2/SEC3/SSA as well as SEB. This would be particularly desirable because toxic shock syndrome caused by *S. aureus* or group A *Streptococci* is difficult to differentiate early on, when antibody treatment would ideally be given.

Our finding has general implications, especially with respect to mAb development for toxin neutralization. In the past, regulatory requirements that necessitated the testing of drugs alone and in combination in patients before licensing added tremendous expense to mAb mixture development. This Food and Drug Administration rule has been revised, and mAb cocktails are in clinical trial for the treatment of *Clostridium difficile* colitis and prophylaxis against rabies (10, 51). Our data further encourage efforts to develop cocktails that include Abs that do not neutralize toxin action directly but instead facilitate clear-

ance. Of note is that the widely advertised investigational treatment for Ebola is also a mixture of three mAbs (52). In viral diseases, the enhancement of combination through Abs is likely critical to rapidly lower pathogen load and the chance of emergence of escape variants. It is conceivable that this concept may also be relevant for mAbs that clear proinflammatory cytokines.

Finally, mAb 20B1 has now also been humanized, and recent data document that this process retained efficacy and nanomolar range affinities (53). The product may be used prophylactically in the event of an imminent threat or immediately after suspected dissemination of SEB before the onset of cytokine storm. Furthermore, based on our data, the product could be used in a multivalent immune-protectant anti-toxin mixture, which should include mAb 14G8. Beyond neutralizing SEB toxin, mAb 20B1 has also been used as adjunctive therapy with antibiotics for treatment of *S. aureus* sepsis (53).

The results of this study established that enhancement of protective efficacy of mAbs through combination of mAbs can have fundamentally different underlying mechanisms. Understanding how combinations of mAbs enhance toxin neutralization will be critical to the production of effective and safe antibody cocktails.

Acknowledgments—We thank the staff of Beamlines X4 and X29 at the National Synchrotron Light Source for assistance in data collection. We thank Prof. Luc Teyton and Dr. Stuart Knowling for providing the TCR-β chain samples. We also thank Dr. John McCormick for providing the SSA toxin and the National Institutes of Health tetramer core facility for MHC class II proteins. We thank Dr. Frank Pessler and Prof. Eckhard Wimmer for critical reading of the manuscript and helpful discussions.

REFERENCES

1. Marrack, P., Blackman, M., Kushnir, E., and Kappler, J. (1990) The toxicity of staphylococcal enterotoxin B in mice is mediated by T cells. *J. Exp. Med.* **171,** 455–464
2. Stiles, B. G., Bavari, S., Krakauer, T., and Ulrich, R. G. (1993) Toxicity of staphylococcal enterotoxins potentiated by lipopolysaccharide: major histocompatibility complex class II molecule dependency and cytokine release. *Infect. Immun.* **61,** 5333–5338
3. Pinchuk, I. V., Beswick, E. J., and Reyes, V. E. (2010) Staphylococcal enterotoxins. *Toxins* **2,** 2177–2197
4. Meddeb-Mouelhi, F., Bouhaouala-Zahar, B., Benlasfar, Z., Hammadi, M., Mejri, T., Moslah, M., Karoui, H., Khorchani, T., and El Ayeb, M. (2003) Immunized camel sera and derived immunoglobulin subclasses neutralizing Androctonus australis hector scorpion toxins. *Toxicon* **42,** 785–791
5. Boucher, P., Sato, H., Sato, Y., and Locht, C. (1994) Neutralizing antibodies and immunoprotection against pertussis and tetanus obtained by use of a recombinant pertussis toxin-tetanus toxin fusion protein. *Infect. Immun.* **62,** 449–456
6. Lomonte, B., León, G., Angulo, Y., Rucavado, A., and Núñez, V. (2009) Neutralization of Bothrops asper venom by antibodies, natural products and synthetic drugs: contributions to understanding snakebite envenomings and their treatment. *Toxicon* **54,** 1012–1028
7. Migone, T. S., Subramanian, G. M., Zhong, J., Healey, L. M., Corey, A., Devalaraja, M., Lo, L., Ullrich, S., Zimmerman, J., Chen, A., Lewis, M., Meister, G., Gillum, K., Sanford, D., Mott, J., and Bolmer, S. D. (2009) Raxibacumab for the treatment of inhalational anthrax. *N. Engl. J. Med.* **361,** 135–144
8. Cheng, L. W., Stanker, L. H., Henderson, T. D., 2nd, Lou, J., and Marks, J. D. (2009) Antibody protection against botulinum neurotoxin intoxication in mice. *Infect. Immun.* **77,** 4305–4313
9. López, E. L., Contrini, M. M., Glatstein, E., González Ayala, S., Santoro, R., Allende, D., Ezcurra, G., Teplitz, E., Koyama, T., Matsumoto, Y., Sato, H., Sakai, K., Hoshide, S., Komoriya, K., Morita, T., Harning, R., and Brookman, S. (2010) Safety and pharmacokinetics of urtoxazumab, a humanized monoclonal antibody, against Shiga-like toxin 2 in healthy adults and in pediatric patients infected with Shiga-like toxin-producing *Escherichia coli*. *Antimicrob. Agents Chemother.* **54,** 239–243
10. Lowy, I., Molrine, D. C., Leav, B. A., Blair, B. M., Baxter, R., Gerding, D. N., Nichol, G., Thomas, W. D., Jr., Leney, M., Sloan, S., Hay, C. A., and Ambrosino, D. M. (2010) Treatment with monoclonal antibodies against *Clostridium difficile* toxins. *N. Engl. J. Med.* **362,** 197–205
11. Demarest, S. J., Hariharan, M., Elia, M., Salbato, J., Jin, P., Bird, C., Short, J. M., Kimmel, B. E., Dudley, M., Woodnutt, G., and Hansen, G. (2010) Neutralization of *Clostridium difficile* toxin A using antibody combinations. *mAbs* **2,** 190–198
12. Chen, C., Wang, S., Wang, H., Mao, X., Zhang, T., Ji, G., Shi, X., Xia, T., Lu, W., Zhang, D., Dai, J., and Guo, Y. (2012) Potent neutralization of botulinum neurotoxin/B by synergistic action of antibodies recognizing protein and ganglioside receptor binding domain. *PLoS One* **7,** e43845
13. Prigent, J., Panigai, L., Lamourette, P., Sauvaire, D., Devilliers, K., Plaisance, M., Volland, H., Créminon, C., and Simon, S. (2011) Neutralising antibodies against ricin toxin. *PLoS One* **6,** e20166
14. Drozdowski, B., Zhou, Y., Kline, B., Spidel, J., Chan, Y. Y., Albone, E., Turchin, H., Chao, Q., Henry, M., Balogach, J., Routhier, E., Bavari, S., Nicolaides, N. C., Sass, P. M., and Grasso, L. (2010) Generation and characterization of high affinity human monoclonal antibodies that neutralize staphylococcal enterotoxin B. *J. Immune Based Ther. Vaccines* **8,** 9
15. Larkin, E. A., Stiles, B. G., and Ulrich, R. G. (2010) Inhibition of toxic shock by human monoclonal antibodies against staphylococcal enterotoxin B. *PLoS One* **5,** e13253
16. Ulrich, R., Sidell, S., Taylor, T. J., Wilhelmsen, C. L., and Franz, D. R. (1997) Staphylocoocal enterotoxin B and related pyrogenic toxins. In *Textbook of Military Medicine: Medical Aspects of Chemical and Biological warfare* (Zajtchuk, R., ed) pp. 621–630, U.S. Department of the Army, The Surgeon General, and the Borden Institute, Washington, D. C.
17. Varshney, A. K., Wang, X., Cook, E., Dutta, K., Scharff, M. D., Goger, M. J., and Fries, B. C. (2011) Generation, characterization, and epitope mapping of neutralizing and protective monoclonal antibodies against staphylococcal enterotoxin B-induced lethal shock. *J. Biol. Chem.* **286,** 9737–9747
18. Tilahun, M. E., Rajagopalan, G., Shah-Mahoney, N., Lawlor, R. G., Tilahun, A. Y., Xie, C., Natarajan, K., Margulies, D. H., Ratner, D. I., Osborne, B. A., and Goldsby, R. A. (2010) Potent neutralization of staphylococcal enterotoxin B by synergistic action of chimeric antibodies. *Infect. Immun.* **78,** 2801–2811
19. Hamad, A. R., Herman, A., Marrack, P., and Kappler, J. W. (1994) Monoclonal antibodies defining functional sites on the toxin superantigen staphylococcal enterotoxin B. *J. Exp. Med.* **180,** 615–621
20. Karauzum, H., Chen, G., Abaandou, L., Mahmoudieh, M., Boroun, A. R., Shulenin, S., Devi, V. S., Stavale, E., Warfield, K. L., Zeitlin, L., Roy, C. J., Sidhu, S. S., and Aman, M. J. (2012) Synthetic human monoclonal antibodies toward staphylococcal enterotoxin B (SEB) protective against toxic shock syndrome. *J. Biol. Chem.* **287,** 25203–25215
21. Alexandrov, A., Dutta, K., and Pascal, S. M. (2001) MBP fusion protein with a viral protease cleavage site: one-step cleavage/purification of insoluble proteins. *BioTechniques* **30,** 1194–1198
22. Davies, J. Q., and Gordon, S. (2005) Isolation and culture of murine macrophages. *Methods Mol. Biol.* **290,** 91–103
23. McCoy, A. J., Grosse-Kunstleve, R. W., Adams, P. D., Winn, M. D., Storoni, L. C., and Read, R. J. (2007) Phaser crystallographic software. *J. Appl. Crystallogr.* **40,** 658–674
24. Lemak, A., Gutmanas, A., Chitayat, S., Karra, M., Farès, C., Sunnerhagen, M., and Arrowsmith, C. H. (2011) A novel strategy for NMR resonance assignment and protein structure determination. *J. Biomol. NMR* **49,** 27–38
25. Sattler, M., Schleucher, J., and Griesinger, C. (1999) Heteronuclear multidimensional NMR experiments for the structure determination of proteins in solution employing pulsed field gradients. *Prog. Nucl. Mag. Res. Sp.* **34,** 93–158

26. Delaglio, F., Grzesiek, S., Vuister, G. W., Zhu, G., Pfeifer, J., and Bax, A. (1995) NMRPipe: a multidimensional spectral processing system based on UNIX pipes. *J. Biomol. NMR* **6,** 277–293
27. Johnson, B. A. (2004) Using NMRView to visualize and analyze the NMR spectra of macromolecules. *Methods Mol. Biol.* **278,** 313–352
28. Pervushin, K. V., Wider, G., and Wüthrich, K. (1998) Single transition-to-single transition polarization transfer (ST2-PT) in [15N,1H]-TROSY. *J. Biomol. NMR* **12,** 345–348
29. Riek, R., Wider, G., Pervushin, K., and Wüthrich, K. (1999) Polarization transfer by cross-correlated relaxation in solution NMR with very large molecules. *Proc. Natl. Acad. Sci. U.S.A.* **96,** 4918–4923
30. Papageorgiou, A. C., Tranter, H. S., and Acharya, K. R. (1998) Crystal structure of microbial superantigen staphylococcal enterotoxin B at 1.5 A resolution: implications for superantigen recognition by MHC class II molecules and T-cell receptors. *J. Mol. Biol.* **277,** 61–79
31. Li, H., Llera, A., Tsuchiya, D., Leder, L., Ysern, X., Schlievert, P. M., Karjalainen, K., and Mariuzza, R. A. (1998) Three-dimensional structure of the complex between a T cell receptor beta chain and the superantigen staphylococcal enterotoxin B. *Immunity* **9,** 807–816
32. Jardetzky, T. S., Brown, J. H., Gorga, J. C., Stern, L. J., Urban, R. G., Chi, Y. I., Stauffacher, C., Strominger, J. L., and Wiley, D. C. (1994) Three-dimensional structure of a human class II histocompatibility molecule complexed with superantigen. *Nature* **368,** 711–718
33. Lehnert, N. M., Allen, D. L., Allen, B. L., Catasti, P., Shiflett, P. R., Chen, M., Lehnert, B. E., and Gupta, G. (2001) Structure-based design of a bispecific receptor mimic that inhibits T cell responses to a superantigen. *Biochemistry* **40,** 4222–4228
34. Scarselli, M., Cantini, F., Santini, L., Veggi, D., Dragonetti, S., Donati, C., Savino, S., Giuliani, M. M., Comanducci, M., Di Marcello, F., Romagnoli, G., Pizza, M., Banci, L., and Rappuoli, R. (2009) Epitope mapping of a bactericidal monoclonal antibody against the factor H binding protein of *Neisseria meningitidis*. *J. Mol. Biol.* **386,** 97–108
35. Xia, T., Liang, S., Wang, H., Hu, S., Sun, Y., Yu, X., Han, J., Li, J., Guo, S., Dai, J., Lou, Z., and Guo, Y. (2014) Structural basis for the neutralization and specificity of Staphylococcal enterotoxin B against its MHC Class II binding site. *mAbs* **6,** 119–129
36. Krautz-Peterson, G., Chapman-Bonofiglio, S., Boisvert, K., Feng, H., Herman, I. M., Tzipori, S., and Sheoran, A. S. (2008) Intracellular neutralization of shiga toxin 2 by an a subunit-specific human monoclonal antibody. *Infect. Immun.* **76,** 1931–1939
37. Smith, M. J., Melton-Celsa, A. R., Sinclair, J. F., Carvalho, H. M., Robinson, C. M., and O'Brien, A. D. (2009) Monoclonal antibody 11E10, which neutralizes shiga toxin type 2 (Stx2), recognizes three regions on the Stx2 A subunit, blocks the enzymatic action of the toxin in vitro, and alters the overall cellular distribution of the toxin. *Infect. Immun.* **77,** 2730–2740
38. O'Hara, J. M., and Mantis, N. J. (2013) Neutralizing monoclonal antibodies against ricin's enzymatic subunit interfere with protein disulfide isomerase-mediated reduction of ricin holotoxin *in vitro*. *J. Immunol. Methods* **395,** 71–78
39. Yermakova, A., Klokk, T. I., Cole, R., Sandvig, K., and Mantis, N. J. (2014) Antibody-mediated inhibition of ricin toxin retrograde transport. *mBio* **5,** e00995
40. Slominska-Wojewodzka, M., Gregers, T. F., Wälchli, S., and Sandvig, K. (2006) EDEM is involved in retrotranslocation of ricin from the endoplasmic reticulum to the cytosol. *Mol. Biol. Cell* **17,** 1664–1675
41. Abboud, N., Chow, S. K., Saylor, C., Janda, A., Ravetch, J. V., Scharff, M. D., and Casadevall, A. (2010) A requirement for FcγR in antibody-mediated bacterial toxin neutralization. *J. Exp. Med.* **207,** 2395–2405
42. Varshney, A. K., Wang, X., Aguilar, J. L., Scharff, M. D., and Fries, B. C. (2014) Isotype switching increases efficacy of antibody protection against staphylococcal enterotoxin B-induced lethal shock and *Staphylococcus aureus* sepsis in mice. *mBio* **5,** e01007–e01014
43. Mukherjee, J., Tremblay, J. M., Leysath, C. E., Ofori, K., Baldwin, K., Feng, X., Bedenice, D., Webb, R. P., Wright, P. M., Smith, L. A., Tzipori, S., and Shoemaker, C. B. (2012) A novel strategy for development of recombinant antitoxin therapeutics tested in a mouse botulism model. *PLoS One* **7,** e29941
44. Sepulveda, J., Mukherjee, J., Tzipori, S., Simpson, L. L., and Shoemaker, C. B. (2010) Efficient serum clearance of botulinum neurotoxin achieved using a pool of small antitoxin binding agents. *Infect. Immun.* **78,** 756–763
45. Ganesan, R., Eigenbrot, C., Wu, Y., Liang, W. C., Shia, S., Lipari, M. T., and Kirchhofer, D. (2009) Unraveling the allosteric mechanism of serine protease inhibition by an antibody. *Structure* **17,** 1614–1624
46. Andersen, L. M., Andreasen, P. A., Svendsen, I., Keemink, J., Østergaard, H., and Persson, E. (2012) Antibody-induced enhancement of factor VIIa activity through distinct allosteric pathways. *J. Biol. Chem.* **287,** 8994–9001
47. Kerschbaumer, R. J., Riedrich, K., Kral, M., Varadi, K., Dorner, F., Rosing, J., and Scheiflinger, F. (2004) An antibody specific for coagulation factor IX enhances the activity of the intrinsic factor X-activating complex. *J. Biol. Chem.* **279,** 40445–40450
48. Yoshihara, E., Gotoh, N., Nishino, T., and Nakae, T. (1996) Protein D2 porin of the *Pseudomonas aeruginosa* outer membrane bears the protease activity. *FEBS Lett.* **394,** 179–182
49. Varshney, A. K., Mediavilla, J. R., Robiou, N., Guh, A., Wang, X., Gialanella, P., Levi, M. H., Kreiswirth, B. N., and Fries, B. C. (2009) Diverse enterotoxin gene profiles among clonal complexes of *Staphylococcus aureus* isolates from the Bronx, New York. *Appl. Environ. Microbiol.* **75,** 6839–6849
50. Mollick, J. A., Miller, G. G., Musser, J. M., Cook, R. G., Grossman, D., and Rich, R. R. (1993) A novel superantigen isolated from pathogenic strains of *Streptococcus pyogenes* with aminoterminal homology to staphylococcal enterotoxins B and C. *J. Clin. Invest.* **92,** 710–719
51. Bakker, A. B., Python, C., Kissling, C. J., Pandya, P., Marissen, W. E., Brink, M. F., Lagerwerf, F., Worst, S., van Corven, E., Kostense, S., Hartmann, K., Weverling, G. J., Uytdehaag, F., Herzog, C., Briggs, D. J., Rupprecht, C. E., Grimaldi, R., and Goudsmit, J. (2008) First administration to humans of a monoclonal antibody cocktail against rabies virus: safety, tolerability, and neutralizing activity. *Vaccine* **26,** 5922–5927
52. Pettitt, J., Zeitlin, L., Kim do, H., Working, C., Johnson, J. C., Bohorov, O., Bratcher, B., Hiatt, E., Hume, S. D., Johnson, A. K., Morton, J., Pauly, M. H., Whaley, K. J., Ingram, M. F., Zovanyi, A., Heinrich, M., Piper, A., Zelko, J., and Olinger, G. G. (2013) Therapeutic intervention of Ebola virus infection in rhesus macaques with the MB-003 monoclonal antibody cocktail. *Sci. Transl. Med.* **5,** 199ra113
53. Varshney, A. K., Wang, X., MacIntyre, J., Zollner, R. S., Kelleher, K., Kovalenko, O. V., Pechuan, X., Byrne, F. R., and Fries, B. C. (2014) Humanized staphylococcal enterotoxin B (SEB)-specific monoclonal antibodies protect from SEB intoxication and *Staphylococcus aureus* infections alone or as adjunctive therapy with vancomycin. *J. Infect. Dis.* **210,** 973–981